Submitted to Physical Review C

LBL-2434
Preprint c.2

EXCITATION OF GIANT MAGNETIC AND SPIN-ISOSPIN DIPOLE STATES IN RADIATIVE π-CAPTURE ON ^{14}N AND ^{10}B

Helmut W. Baer, James A. Bistirlich, Nico de Botton,
Susan Cooper, Kenneth M. Crowe, Peter Truöl, and John D. Vergados

August 1974

Prepared for the U.S. Atomic Energy Commission
under Contract W-7405-ENG-48

LBL-2434

DISCLAIMER

EXCITATION OF GIANT MAGNETIC AND SPIN-ISOSPIN DIPOLE STATES IN RADIATIVE π-CAPTURE ON ^{14}N AND ^{10}B†

Helmut W. Baer,* James A. Bistirlich, Nico de Botton,‡
Susan Cooper, and Kenneth M. Crowe

Lawrence Berkeley Laboratory
University of California
Berkeley, California 94720

and

Peter Truöl

Physik-Institut de Universität Zürich
Zürich, Switzerland

and

John D. Vergados

Department of Physics
University of Pennsylvania
Philadelphia, Pennsylvania

August 1974

ABSTRACT

The photon spectra in the capture of stopped pions on ^{14}N and ^{10}B were measured in the 50-150 MeV region with a high-resolution pair spectrometer. The total radiative capture branching ratios are $2.13 \pm 0.21\%$ and $2.27 \pm 0.22\%$, respectively. The spectrum corresponding to the first 13 MeV excitation in each of the residual nuclei, ^{14}C and ^{10}Be, is dominated by the transition to the analog of a giant M1 state of the target nucleus. The ground state transitions in both nuclei are resolved experimentally. The measured branching ratio for the extremely weak ^{14}C(g.s.) transition is $(3 \pm 2) \times 10^{-5}$. There is evidence for selective excitation of the analogs of the giant dipole spin-isospin states of ^{14}N, of which the 3^- component appears to be the strongest. In ^{10}B the transition strength to the giant resonance region is more fragmented. An

analysis is presented that employs an impulse-approximation Hamiltonian with amplitudes taken directly from the fundamental process on the nucleon, $\pi^- + p \rightarrow n + \gamma$, and shell-model wave functions obtained using realistic interactions in the 1s, 1p, and 2s-1d shells. Also, a calculation for the ^{14}C(g.s.) transition from 1s capture using the "elementary-particle soft-pion" ansatz is presented.

I. INTRODUCTION

Within the last several years the (π^-, γ) reaction with stopped pions was found to be a good probe of nuclear structure. Among the measurements which demonstrated this were those on targets of ^{3}He (Ref. 1), ^{4}He (Ref. 2), ^{6}Li (Ref. 3). ^{12}C (Ref. 4), ^{16}O (Ref. 5), and ^{209}Bi (Ref. 6) in which the photon spectrum between 50 and 150 MeV was measured with a pair spectrometer of 2-MeV resolution. These data and their interpretations have established the general features of this reaction, which can be summarized briefly as follows:

(1) The total radiative branching ratio for the direct transitions producing high-energy photons on nuclei with $A \geq 4$ ranges from 1% (^{209}Bi) to 4.4% (^{6}Li), with most measured values near 2%.

(2) The largest fraction (70-90%) of the photons are associated with quasi-free capture on a proton, i.e., $\pi^- + A \rightarrow (A-1) + n + \gamma$, which produces a continuum spectrum with a maximum between 110 and 120 MeV, falling off sharply at the high-energy end, near 135 MeV, and extending down below 50 MeV.

(3) Strong and selective excitations of unbound states in the energy region of the giant dipole resonance (GDR) built on the target nucleus were observed in ^{12}C. Since the (π^-,γ) transition operator contains the nucleon spin, these excitations have generally been interpreted[7] as spin-isospin dipole vibrations characterized by $L = 1$, $S = 1$, $J^\pi = 0^-, 1^-, 2^-$, $T = 1$, and $T_z = +1$ in the SU(4) classification[8] of giant resonances. These spin-isospin vibrations are distinct from the isospin modes ($L = 1$, $S = 0$, $T = 1$) excited in E1 photoexcitation which involve no spin change. In ^{12}C both 1^- and 2^- states were strongly excited in (π^-,γ) (Ref. 4). The identification of the 1^- component as a spin-isospin vibration mode is not without ambiguity, however, since its energy coincides with the energy of the 1^- states observed in E1 photoexcita-

tion. In other nuclei, e.g. ^{16}O, no narrow resonance-like peaks were observed in the GDR region, whereas they clearly exist in photoexcitation reactions.

(4) Transition strengths to the particle stable states and low-continuum states (below the GDR) on targets of ^{3}He, ^{6}Li, ^{12}C, and ^{16}O exhibit one strong, dominating transition. The transitions $^{6}Li(\pi^{-},\gamma)^{6}He(g.s.)^{3}$ and $^{3}He(\pi^{-},\gamma)^{3}H(g.s.)^{1}$ have served as test cases in the theoretical analyses. For the heavier targets the level density in the residual nuclei, ^{12}B and ^{16}N, is so large compared to the 2-MeV experimental resolution that the strong transition could not be assigned to a single state. Theoretical arguments favored the identification[5] of much of the strength with the 1^{+} and 2^{-} ground states, respectively.

(5) The general utility of the (π^{-},γ) reaction for structure studies on nuclei with $A>16$ has not been firmly established. In the ^{24}Mg and ^{40}Ca data[5] sharp lines were not observed. However, the recently completed study on $^{209}Bi(\pi^{-},\gamma)^{209}Pb$ (Ref. 6) shows some evidence for excitation of a sharp line.

Theoretical interpretations of these data have proceeded along two lines. PCAC and soft-pion theorems have been applied[9] to calculate transitions in ^{3}He and ^{6}Li. In the soft-pion limit, the (π^{-},γ) reaction is governed by the matrix element of the weak axial-vector current, and thus it can be related to Gamow-Teller β-decay and the axial-vector matrix elements of μ-capture. By introducing assumptions about the dependence of the form factors on momentum transfer, several authors[9] predicted (π^{-},γ) rates from the experimental weak-interaction matrix elements. Such calculations for ^{3}He and ^{6}Li and compare[1,3] reasonably well with the data. A limitation of this approach is that it holds only for 1s-capture. For nuclei with $4 \leq A \leq 40$, p-state capture accounts for more than 50% of π-absorption.

The second approach, which has a wider applicability to nuclear structure studies, makes use of an impulse approximation (IA) Hamiltonian determined directly from the fundamental photo-pion production process, $\pi^- + p \rightleftarrows n + \gamma$. This is applied without adjustment of parameters to calculate the (π^-, γ) rates in complex nuclei described by shell-model wave functions. In ^{6}Li this has led to excellent agreement[3] with the most recent data.

To make further advances in $(\pi^-\gamma)$ nuclear structure studies, several factors seemed important. First, there was need for measurements on several additional transitions where a single nuclear state was isolated experimentally. ^{10}B and ^{14}N are the only nuclei where this is possible with a resolution of 2 MeV. The first excited state of the residual nucleus ^{14}C is at 6.1 MeV; in ^{10}Be the first and second excited states are at 3.4 and 6.0 MeV. Furthermore, since the target ^{10}B has $J^\pi = 3^+$, whereas all other light nuclei studied had $J^\pi = 0$, $1/2^+$, or 1^+, the dependence on angular momentum could be further investigated.

Second, the further clarification of the role of giant M1 states in (π^-, γ) reactions was of interest. In 1963 Kurath[10] suggested that in light nuclei there exists a concentration of magnetic dipole transition strength between T = 0 ground states and excited T = 1 states similar to the well known concentration of E1 strength in the GDR. The most direct observation of such giant M1 states was expected[10] to be in 180° electron scattering, and indeed prominent M1 transitions have been observed[11] in ^{6}Li, ^{10}B, ^{12}C, ^{14}N, ^{20}Ne, ^{24}Mg, ^{28}Si and other nuclei. In recent years Mukhopadhyay[12] suggested that μ-capture from atomic 1s orbits exhibits concentration of transition strength to the giant M1 states because the dominant part of the transition operator resembles the Gamow-Teller (GT) interaction. Experimental verification in μ-capture has been limited and must necessarily be indirect, e.g., through

observation of secondary and tertiary γ and β rays, since the neutrino emitted in the primary transition cannot be detected. Radiative pion capture, however, provides an excellent method for further exploring these giant M1 states. since radiative π-capture transitions from $\ell = 0$ atomic orbits are essentially governed by the same GT matrix elements $\int \vec{\sigma}\tau^+$ that appear in μ-capture and β-decay. A complication arises in π-capture, not existing in μ-capture, in that π's are captured predominantly from p orbits in light nuclei ($\sim$ 90% for ^{14}N). In this case the $\vec{q}$-dependent terms of the interaction make large contributions[13] to the radiative capture rate. However, this effect does not significantly change the above results because, when the pion momentum operator $\vec{q} = -i\vec{\nabla}$ operates on the 2p pion wave function, it yields both a monopole (essentially the GT operator) and a quadrupole term. The contribution of the quadrupole term is negligible[13] (precisely for the same reasons that the momentum-dependent terms are negligible for 1s absorption). As a result, the role of the GT operator is much greater than expected from the 10-20% 1s state capture probabilities. Thus the (π^-,γ) reaction appeared to be a promising means for observing the analogs of the well-known[11] giant M1 states in ^{10}B at 7.48 MeV and in ^{14}N at 9.2 and 10.4 MeV.

A third area of interest was the (π^-,γ) excitation of collective states in the GDR region. The comparison of the distribution of (π^-,γ) transition strength with that of photoexcitation and electron scattering might elucidate the spin-isospin structure of the GDR. The spin-isospin modes of ^{10}B have $J^\pi = 1^-, 2^-, 3^-, 4^-$, and 5^- and in ^{14}N have $J^\pi = 0^-, 1^-, 2^-$, and 3^-. We hoped to obtain evidence for some of these higher spin components which cannot be easily observed in other reactions. Our study presents some evidence for such excitations in ^{14}N.

II. EXPERIMENT

The experiment was performed in the stopped-π^- channel of the Lawrence Berkeley Laboratory 184 in. cyclotron (Fig. 1). A π^- beam of 180 MeV/c, extracted from an internal Be production target by the cyclotron fringe field, is brought to a focus 10 m from production by a quadrupole-dipole-quadrupole magnet system. Maximum achieved beam intensity was 2×10^6 π^-/sec with a circular spot size of ~ 8 cm diameter and $\Delta p/p \approx 13\%$ (full width). The π^- were brought to rest in targets of liquid nitrogen (15.2 cm diameter, 5.1 cm long cylindrical flask) and 91.4%-enriched ^{10}B power ($11.3\times13.9\times5.1$ cm^3 parallelepiped, 941 g mass). Typical stopping rates were $(2\text{-}3)\times10^5$/sec. The photons were detected in a 180° pair-spectrometer (Fig. 1, also Refs. 3 and 5) employing a 3% radiation length gold foil (0.22 g/cm^2) converter. The momenta of the e^+-e^- pair were determined by measuring their trajectories in a magnetic field ($B_{max} \approx 8.3$ kG) with three wire spark chambers. Each chamber consisted of four wire planes with seven magnetostrictive-wire delay-line readouts. The wire spacing was 0.1 cm and the wire angles with the horizontal midplane of the magnet were +12, -12, -12, and 0°. A PDP-15 computer was used on-line to record the data onto magnetic tape and to monitor the performance of the spark chambers. The acceptance (conversion $\times\Delta\Omega/4\pi\times$ detection efficiency) of the spectrometer as a function of photon energy (Fig. 2a) was determined with a Monte Carlo calculation which includes the experimental geometry, a field map, pair-production cross sections, energy loss due to radiation and ionization, and multiple scattering in the converter and chambers.

Numerous runs with a liquid hydrogen target were taken during the course of the experiment to check the performance of the spectrometer. A spectrum is shown in Fig. 2b. The 129.41-MeV photon of the $\pi^- + p \rightarrow n + \gamma$ reaction gives the instrumental line shape, and it is seen that 2-MeV resolution (fwhm) was achieved. The peak of the line shape is shifted downward by ~ 2 MeV

from the photon energy due to energy loss of the e^+-e^- pair in the converter and spark chambers. The charge-exchange capture, $\pi^- + p \rightarrow n + \pi^\circ$; $\pi^\circ \rightarrow 2\gamma$, provides, via the Panofsky ratio, a check on the relative acceptance in the region $54.9 < E_\gamma < 83.0$ MeV. The modification of the rectangular π° spectrum by the acceptance curve can be observed.

The 5 - 10% good events of the total triggers were selected with an off-line pattern recognition program; the different classes of background events are described in Ref. 5. The efficiency for finding good events was determined by examining 50,000 triggers by eye in a direct display of the spark chamber coordinates. The program detection efficiency was $53 \pm 3\%$ at 130 MeV with a small additional bias against lower-energy events. The spectrometer acceptance at 130 MeV is $\eta(130) = (\text{conversion} \times \Delta\Omega/4\pi) \times (\text{detection efficiency})$ $= (4.15 \times 10^{-5})\ (0.532) = (2.21 \pm 0.12) \times 10^{-5}$.

The number of pions stopping in each target was obtained in two ways. First, the fraction of incident π's stopping in the target was determined from target in/out measurements. In this way π's stopping in the target walls as well as geometric and electronic inefficiencies are taken into account; also, this method was checked with equivalent-geometry CH_2 targets and measured CH_2 range curves. Second, the stopping fraction was calculated from the equivalent CH_2 stopping power of the targets and measured CH_2 range curves. The two methods were generally in agreement to within 6%.

The radiative branching ratio for a single peak or the entire spectrum (total radiative branching ratio) is determined by use of the expression

$$R_\gamma = \frac{N_\gamma \cdot (1 - \ell) \cdot t \cdot e^{\mu x}}{\pi_{in} \cdot \epsilon \cdot (1 - \delta) \cdot \eta(130)}$$

N_γ is the number counts in the spectrum after eliminating, through target cuts, events originating outside the target; ℓ represents the small fraction of counts resulting from radiative in-flight transitions; t is the unfolding

factor which multiplies $N_\gamma(1 - \ell)$ to give the number of photons expected with a uniform spectrometer acceptance at the value $\eta(E_\gamma = 130\ \text{MeV})$. For a single peak, $t = \eta(130)/\eta(E_\gamma)$. For R_γ (total) it is determined by folding the pole-model distribution function (Sec. IIIA) with the spectrometer acceptance and line shape (Fig. 1) and comparing the result with the spectrum. The fraction of the photons with energies below 50 MeV, and thus not observed in the pair spectrometer, is 3-5% as given by the pole model. $e^{\mu x}$ corrects for the attenuation of photons in the target, scintillation counter, and spark chamber between the converter foil and origin. $\pi_{in} \cdot \epsilon \cdot (1 - \delta)$ is the number of pionic atoms formed as determined from the particles passing through the three upstream counters of the telescope (π_{in}), the π-stopping fraction ϵ, and the small corrections for nonradiative in-flight interactions (estimated ~ 1%).

III. EXPERIMENTAL RESULTS

A. General

In-flight subtraction. The photon spectra for π^- capture on ^{14}N and ^{10}B are displayed in Figs. 3 and 4. From the raw data, Figs. 3a and 4a, one sees that there are a few counts at energies above the kinematically allowed region for stopped-π reactions. The trajectory reconstructions indicate that these photons emanate from the target, and we identify them with in-flight radiative capture (REX), $\pi^- + A_Z \rightarrow A_{Z-1} + \gamma$ and in-flight charge exchange (CEX), $\pi^- + A_Z \rightarrow A_{Z-1} + \pi^\circ, \pi^\circ \rightarrow 2\gamma$. From the range curve data we can see that π's with kinetic energies up to ~ 35 MeV were entering both the ^{14}N and ^{10}B targets. For $T_\pi = 35$ MeV, REX photons up to ~ 173 MeV can be produced. CEX photons from the decay of a 35-MeV π° range from 32 to 140 MeV.

The in-flight spectrum (Fig. 3b) at 90° to the beam was measured with the ^{14}N target at $T_\pi = 44 \pm 7$ MeV (the lowest energy consistent with not having π's stop in the target). It is rather featureless, in agreement with the

expected dominance of the CEX reaction as discussed below. By normalizing this in-flight spectrum to the stopped-π spectra between 140 and 150 MeV, we find a $10 \pm 3\%$ and $6 \pm 2\%$ subtraction necessary for ^{14}N and ^{10}B, respectively. The resulting spectra are shown in Figs. 3c and 4b.

The cross sections for in-flight processes on nuclei at these low beam energies have not been measured. Clearly[14] they do not exceed $Z\times$(free proton cross section). These are for CEX[15] $\sigma_0(^{14}N) = 7 \times 5.25 = 36.8$ mb and for REX[16] $\sigma_\gamma(^{14}N) = 7 \times 1$ mb. Here we have used nucleon cross sections at $T_\pi = 15$ MeV, which we estimate to be the average energy for π's interacting in flight in the ^{14}N target. To calculate from these cross sections the expected in-flight contributions to the total spectrum, we assumed that the CEX photon distribution was rectangular and that the REX spectrum was similar to the stopped-π spectrum. To check the shape of the CEX spectrum, a calculation[17] was performed for the in-flight photon spectrum at 90° to the beam using π° angular distributions of $1 \pm \cos\theta$. These produced shapes very close to rectangular. Little is known about the shape of the in-flight REX spectrum. However, since we calculate that its contribution is small, our assumption should not lead to a significant error in the estimate of the total in-flight contribution. With these assumptions, we estimate upper limits for the in-flight contributions to the stopped-π spectrum of 13% for CEX and 4.3% for REX.

It is well known[14] that $Z\times$(free proton cross section) overestimate the nuclear cross sections, since no account is made of pion attenuation and binding energy effects. In a measurement at 70 MeV on ^{12}C, Hilscher et al.[18] found a reduction factor of 48% on $Z\times$(free proton cross section) for the CEX reaction on ^{12}C. This factor is consistent with the cross sections deduced from our in-flight data at $T_\pi = 44$ MeV, to within the uncertainty (up to factor of 2) resulting from our lack of knowledge on the π° energy distribution. Thus

we conclude that our in-flight subtraction is in reasonable agreement with the expected in-flight contribution.

Quasi-free capture. In nuclei ranging from ^{3}He to ^{209}Bi, the quasi-free component [$\pi^- + A \rightarrow (A - 1) + n + \gamma$] is well described phenomenologically by the pole model.[19] The one-pole diagram and the calculated γ-spectrum are shown in Figs. 3c and 4b. Details of the model and the expression for the spectrum are given in Ref. 20. The normalization and the average excitation energy ($E^* = \Delta - \Delta_{min}$; $\Delta_{min} = M_{A-1} + m_n - M_A$) of the recoil nucleus are not specified in this model, so our procedure has been to determine them by fitting to the data between 70 and 110 MeV. This region should be free of nuclear resonances. For ^{14}N (Δ_{min} = 8.5 MeV), values E^* = 4.5 - 5.5 MeV and for ^{10}B (Δ_{min} = 7.9 MeV) values E^* = 5.1 - 6.1 MeV give good descriptions of the data.

In the spectrum of ^{14}N one can see a resonance-like peak at ~ 20 MeV in ^{14}C, which is the region of the GDR. A similar resonance cannot be clearly discerned in the spectrum of ^{10}B. To extract a value for the branching ratio to the GDR region in the ^{14}N spectrum, a Breit-Wigner (BW) form superimposed on the pole-model continuum was fit to the data. Clearly the extracted transition fractions (Table I) in such an analysis are model dependent, since the separation between the pole model and resonance excitation is not well defined. A shell-model analysis and more discussion of the giant resonance region in ^{14}C is presented in Section IVD.

B. Results on ^{14}N

The total and partial radiative branching ratios determined for ^{14}N are given in Table I. The quasi-free fraction of the total radiative branching ratio $R_\gamma = 2.13 \pm 0.21\%$, as given by the pole model (Δ = 13.5, Fig. 3d), is $83 \pm 2\%$. An additional 10% of the strength is attributed to GDR excitation as

described by the BW, leaving only 7% for the particle-stable and low-continuum states.

E_x = 0-13 MeV. The data on the first 13-MeV excitation of ^{14}C, after subtraction of the pole-model and BW contributions as shown in Fig. 3d, are shown on an expanded scale in Fig. 5. From previous work[21] it is known that at least 15 levels occur in this region. Of these, it is possible to identify two with little ambiguity in the (π^-, γ) reaction. The ground state is separated by 6.09 MeV from the first excited state; the measured branching ratio is $(3 \pm 2) \times 10^{-5}$. A strong transition is observed at E_γ = 131 MeV, and a single-line fit yields $E_x = 7.0 \pm 0.3$ MeV, which agrees closely with the 7.01 ± 0.01 MeV measured[21] previously for the 2_1^+ state.

To analyze the remaining transition strength we must be guided by previous experiments and theory. Previous (π^-, γ) studies on ^6Li (Ref. 3) and ^{12}C (Ref. 4), together with the present work, show that the strongest transitions are to states whose analogs in the target nucleus have the largest M1 matrix elements with the ground state. Specifically, in the earlier studies the dominating transitions were to $^6He(g.s., 0^+)$ and $^{12}B(g.s., 1^+)$, which are the $T_z = +1$ analogs of the 3.56-MeV state in ^6Li and 15.1-MeV state in ^{12}C. Both states are observed strongly in 180° electron scattering and have large measured M1 matrix elements. In $^{14}N(e,e')$, the largest observed[22] M1 rates are to 2^+ states at 9.17 and 10.43 MeV. The analogs in ^{14}C occur at 7.0 and 8.3 MeV, respectively. Our data are consistent with population of both of these states with the 7.0-MeV state strongest (Fig. 5).

Additional transition strength is seen at 10-13 MeV excitation. Unfortunately, the ^{14}N (e,e') studies were not extended to this excitation region. Preliminary results[11] on $^{14}C(e,e')$ indicate that a 1^+ state at 11.3 MeV has considerable M1 strength to the ^{14}C ground state. These data establish the J^π,

but do not guarantee a large M1 matrix element for the analog state in ^{14}N, since different ground states are involved. A 1^+, T = 1 state in ^{14}N was identified[23] at 13.72 MeV in the $^{15}N(^3He, \alpha)^{14}N$ reaction, and perhaps this is the analog of the state observed in $^{14}C(e,e')$.

Taking into account these various results, we fit the data on the first 14-MeV excitation in ^{14}C with four lines at 0.0, 7.0, 8.3, and 11.3 MeV. The results are displayed in Fig. 5 and the corresponding branching ratios given in Table I.

GDR region. The GDR built on the ^{14}N ground state has been studied through photoexcitation[24] and radiative proton capture $^{13}C\ (p,\gamma)^{14}N$ (Ref. 25). The total photoabsorption cross section shows a rather smooth energy dependence compared to other 1p shell nuclei,[26] e.g., ^{12}C and ^{16}O, with a peak near 22 MeV and a considerable tail at higher energies. The $^{13}C(p,\gamma)^{14}N$ excitation function shows a broad structure in the region $18 \lesssim E_x \lesssim 24$ MeV, with prominent peaks at E_x = 22.5 and 23.0 MeV. The analogs in ^{14}C are expected at E_x = 20.1 and 20.6 MeV. These energies are close to the 20 ± 1 MeV for the position of the BW peak determined in this experiment.

In the $^{13}C(p,\gamma_0)^{14}N$ study, the γ_0 angular distribution was thought[25] to be consistent with $J^\pi = 2^-$ for most of the observed giant electric dipole strength. The results of our shell-model calculations (Section IV) indicate that the strongest transitions in the $^{14}N(\pi^-,\gamma)^{14}C$ reaction are to 3^- states, with some strength also to 2^- states. If indeed the giant 3^- states are seen in the present experiment, some major 2^- and 3^- components of the GDR are nearly degenerate, since the measured excitation energies in the two experiments are so close. This differs from ^{12}C, where the major 1^- and 2^- components are separated by about 3.5 MeV and could be resolved in the $^{12}C(\pi^-,\gamma)$ experiment.[4]

C. Results on ^{10}B

The total and partial radiative branching ratios determined for ^{10}B are given in Table II. The quasi-free fraction of the total radiative branching ratio $R_\gamma = 2.27 \pm 0.22\%$, as given by the pole-model, is $87 \pm 4\%$.

E_x = 0-13 MeV. The data on the first 13-MeV excitation of ^{10}Be, after subtraction of the pole-model contribution as shown in Fig. 4c, are displayed on an expanded scale in Fig. 6. Previous experiments[27] established that the first three states of ^{10}Be have $J^\pi = 0^+$, 2_1^+, and 2_2^+ and the energies are 0, 3.37, and 5.96 MeV, respectively; the analogs in ^{10}B are at 1.74, 5.11, and 7.477 MeV. The three additional particle stable states[27] (1^-, 0^+, 2^-) of ^{10}Be are within 0.3 MeV of the 2_2^+ state. With our resolution of 2 MeV the ground state can be resolved, and evidence for its population is clearly seen in the spectrum. The strongest transition occurs at $E_\gamma \approx 132$ MeV, and a single line fit yields $E_x = 6.0 \pm 0.3$ MeV, which agrees closely with the previous value for the 2_2^+ state. The analog of this state is strongly excited in $^{10}B(e,e')$,[28] and its M1 strength is by far the largest measured in ^{10}B. The calculations by Mukhopadhyay[12] for μ-capture, using the Cohen-Kurath wave functions, indicate that this 2^+ state receives 62% of the transition strength to states with $(p\,1/2,\ p\,3/2)^6$ configuration. Thus it seems reasonable to assume that the peak at ~ 132 MeV is mostly due to the 2_2^+ state, and that the other three states make much smaller contributions. The data also show population of the 2_1^+ state, since only it can account for the observed filling in of counts between the ground state and the 2_2^+ state. A fit of three lines with energies fixed at the first three ^{10}B states gives a good description to the data. The three extracted branching ratios (Table II) are expected to be quite free of uncertainties due to background and level population ambiguities, and thus they should provide good test cases for theoretical calculations.

Additional transition strength is observed to states between 8 and 12 MeV. Not much is known experimentally about levels in this region. The calculations by Mukhopadhyay[12] for μ-capture predict relatively strong excitation (21%) of a 3^+ state at 8.9 MeV and weaker (4.1%) excitation of a 4^+ state at 10.8 MeV (energies are theoretical estimates). Our calculation (Section IV) for π-capture predicts that the strongest excitations to this region are a 2^+ state and a 4^+ state. Other states are predicted to be much weaker in both μ- and π-capture. Noting these results, we fit two lines to the remaining transition strength, allowing both the energies and intensities to vary (Table II).

GDR region. The GDR region of ^{10}B has been investigated by photo excitation[29] and radiative proton capture ^{9}Be(p,γ)^{10}B,[30] but not in (e,e'). The photo-absorption[29] cross sections show two peaks at 20.1 ± 0.1 MeV and 23.1 ± 0.1 MeV. The analogs in ^{10}Be are expected at ~ 18.7 MeV and 21.7 MeV. Regarding the spin-parity structure, little is known, except that since ^{10}B has a 3^+ ground state, states seen strongly in E1 photo-absorption must have $J^\pi = 2^-$, 3^-, or 4^-. The ^{10}B(π,γ) data show little resolved structure in the GDR, and no clear separation between quasi-free and resonance capture can be ascertained. Since other 1p shell nuclei clearly show strong (π^-,γ) transitions to the GDR region, it seems probable that this also occurs in ^{10}B, but that there is greater fragmentation of the strength.

IV. SHELL-MODEL STUDIES

A. General

Calculation of the radiative π-capture transition probabilities requires essentially three ingredients: the effective interaction responsible for the transition, specification of the bound pion wave function, and appropriate nuclear wave functions. To deduce branching ratios from the transition rates, one also needs pionic capture schedules and strong absorption level widths.

Each of these subjects is discussed below.

1. The (π^-, γ) interaction

Using the CGLN[31] photo-pion production amplitude, Delorme and Ericson[32] write the effective Hamiltonian with the pion in the $\phi_\ell^n(\vec{r})$ atomic orbit as

$$\mathcal{H}_{eff} = \left(1 + \frac{m_\pi}{m_p}\right) \sum_{j,\lambda}^{A} e^{-i\vec{k}\cdot\vec{r}_j} H_\lambda(j)\, \phi_\ell^n(\vec{r})\, \delta(\vec{r}-\vec{r}_j), \qquad (1)$$

where

$$H_\lambda(j) = 2\pi i t^+(j)\Big[A\vec{\sigma}_j\cdot\hat{\epsilon}_\lambda + B(\vec{\sigma}_j\cdot\hat{\epsilon}_\lambda)(\vec{q}\cdot\vec{k}) + C(\vec{\sigma}_j\cdot\vec{k})(\vec{q}\cdot\hat{\epsilon}_\lambda)$$

$$+ iD\,\vec{q}\cdot(\vec{K}\times\hat{\epsilon}_\lambda) + E(\vec{\sigma}_j\cdot\vec{q})\ (\vec{q}\cdot\hat{\epsilon}_\lambda)\Big] \qquad (2)$$

in the notation of Ref. 13. The first term in $H_\lambda(j)$ accounts for nearly all the transition strength in s-state capture; for p-state capture the terms linear in $\vec{q}$ make large contributions.[13] The E-term, quadratic in $\vec{q}$, is not expected to make significant contributions to s- and p-state capture.

The effective coupling constants A, B, C, D, and E are linear combinations of the electric and magnetic multipole amplitudes contributing to the $\gamma + n \rightarrow \pi^- + p$ cross section at low energies. Threshold values have been given by numerous authors.[33] Although the most recent solutions (1972-73) are all based on the tables of Berends et al.[34] (1967), there are still some discrepancies in B, C, D, and E. Our calculations were performed with the values of Maguire and Werntz, including the sign change in the D-term.[35] The effect of using other values was investigated for several transitions and was found to be small.

2. The pionic orbits

A great advantage of the (π^-, γ) reaction with stopped pions is that the π's initial state is a bound atomic orbit which can be studied through the pionic x-ray spectra. The pionic wave functions can be obtained by solving[36] the

Klein-Gordon equation in the potential generated by the nucleus. Such solutions show that the hydrogenic wave functions are distorted by the strong interaction of the π^- with the nucleus and the finite nuclear size. However, since both the hydrogenic and the distorted s- and p-wave functions vary relatively slowly inside the nucleus, one can use hydrogenic wave functions and an appropriate scale factor $C_{n\ell}$, $\Lambda_\gamma(n\ell$, optical potential) = $C_{n\ell}\Lambda_\gamma(n\ell$, hydrogenic). The $C_{n\ell}$ can be determined from

$$C_{n\ell} = \frac{\langle NL \mid \phi^\pi \text{ (opt.pot.)} \mid NL\rangle^2}{\langle NL \mid \phi^\pi \text{ (hydrogenic)} \mid NL\rangle^2}, \tag{3}$$

where NL are the shell-model single-particle states. Values of $C_{1s} = 0.5$ and $C_{2p} = 1.4$ were used for both ^{10}B and ^{14}N. These values were determined by Maguire and Werntz[35] for ^{12}C by comparing pion wave functions based on the optical model of Krell and Ericson[36] with hydrogenic wave functions.

3. Nuclear wave functions

The nuclear wave functions were calculated with standard shell-model techniques (c.f.p. and Racah algebra) using harmonic oscillator wave functions with $\hbar\omega$ = 14 MeV. The (π^-,γ) rates are known[13,35] to be sensitive to the value of $\hbar\omega$ adopted. The present value, derived from considerations of the energy spectrum of the nuclei around ^{16}O, is consistent with electron scattering experiments which yield $\langle r^2\rangle^{1/2}$ = 2.58 F ($\hbar\omega$ = 13.7 MeV) for the 1p-shell harmonic-oscillator length parameter. The single-particle energies[37] were taken from experiment. Positive parity states were calculated in a $(1p_{3/2}\ \ 1p_{1/2})^n$ space with n = - 2 for ^{14}N and n = 6 for ^{10}B. Higher shell admixtures play an important role for some states (e.g., 2_1^+ in ^{14}N) as will be discussed. For negative parity states (calculated only for ^{14}N), one particle

was promoted from the 1s to 1p shell or from the 1p to 2s-1d shells. Pictorially, the model space for ^{14}N is

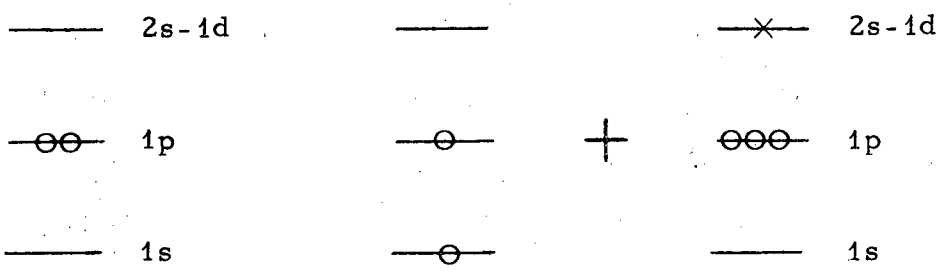

+ parity - parity

It is expected that if the ground states of ^{10}B and ^{14}N are well described by $(1p_{3/2}, 1p_{1/2})^n$, more complex excitations will not affect the total π^- capture rate to either positive or negative parity states, but may affect the distribution of strength among the different states.

The basic states were allowed to mix with a realistic two-body interaction obtained from the bare G-matrix elements of Kuo and Lee,[38] a somewhat modified version of the earlier matrix elements of Kuo and Brown.[39] The bare interaction, however, requires fairly large Hilbert spaces. Therefore some calculations were also performed with the effective interaction of Cohen and Kurath[40] with their set of single-particle energies, and some comparisons are given below.

4. Branching ratios

The transition probabilities are given by

$$\Lambda_\gamma(n\ell;\, J_i \to J_f) = \frac{k}{\pi}\,\frac{1}{2J_i+1}\,\frac{1}{2\ell+1}\,S_{i\to f}\,, \tag{4a}$$

$$S_{i\to f} = \int \frac{d\hat{k}}{4\pi} \sum_{m's} |\langle J_f M_f |\mathcal{H}_{eff}| J_i M_i\rangle|^2 . \tag{4b}$$

The branching ratio R_γ, i.e., the number of photons per stopped pion, is related to $\Lambda_\gamma(n\ell)$ as follows:

$$R_\gamma = \sum_{n,\ell} \frac{\Lambda_\gamma(n\ell)}{\Lambda_a(n\ell)}\ \omega(n\ell) \tag{5}$$

where $\Lambda_a(n\ell)$ are the total absorption rates and $\omega(n\ell)$ are the probabilities for absorption from orbit $n\ell$. The latter are restricted by the condition $\sum_{n,\ell} \omega(n\ell) = 1$ which expresses the fact that the nuclear absorption lifetimes are much shorter than the free-pion lifetimes ($10^{-12} << 2.8 \times 10^{-8}$ sec). It is generally assumed[35] that the ratio $\Lambda_\gamma(n\ell)/\Lambda_a(n\ell)$ depends only on ℓ, not n. In light nuclei, capture occurs only from $\ell = 0$ and $\ell = 1$ orbits, thus the quantity

$$R_\gamma = R_s + R_p = \frac{\Lambda_\gamma(1s)}{\Lambda_a(1s)}\ \omega_s + \frac{\Lambda_\gamma(2p)}{\Lambda_a(2p)}\ \omega_p \tag{6}$$

is compared to experiment. The quantities $\omega_s = \sum_n \omega(ns)$ and $\omega_p = \sum_n \omega(np)$ have not been obtained for ^{10}B or ^{14}N, but extrapolating from[41] ^{6}Li, ^{9}Be, ^{12}C, and ^{16}O, it appears that $\omega_s = 0.20 \pm 0.05$ for ^{10}B and $\omega_s = 0.10 \pm 0.03$ for ^{14}N are reasonable and these were used ($\omega_p = 1 - \omega_s$). The total absorption rates were taken[42] to be: for ^{14}N, $\lambda_a(1s) = 4.48 \pm 0.30$ keV/$\hbar$ $= (6.82 \pm 0.46) 10^{18}$ sec^{-1} $\lambda_a(2p) = 2.1 \pm 0.3$ eV/$\hbar$ $= (3.19 \pm 0.46)\ 10^{15}$ sec^{-1}; for ^{10}B, $\lambda_a(1s) = 1.68 \pm 0.12$ keV/$\hbar$ $= (2.55 \pm 0.18)\ 10^{18}$ sec^{-1} and $\lambda_a(2p) = 0.32 \pm 0.06$ eV/$\hbar$ $= (0.487 \pm 0.091) 10^{15}$ sec^{-1}.

B. Positive Parity States of ^{14}N

Although the eigenstates were originally obtained in the j-j coupling scheme, it is more instructive to examine the positive parity states in the LS representation. The states of interest are:

^{14}N(g.s.): $|1^+, T=0\rangle = 0.1636\ |\ L=0\ S=1\rangle + 0.9564 |L=2\ S=1\rangle + 0.2420 |L=1\ S=0\rangle$

^{14}C(g.s.): $|0^+, T=1\rangle = 0.7980\ |\ L=0\ S=0\rangle + 0.6027 |L=1\ S=1\rangle$

5.1 MeV : $|2^+_1, T=1\rangle = 0.9068\ |\ L=2\ S=0\rangle - 0.4216 |L=1\ S=1\rangle$

7.1 MeV : $|1^+, T=1\rangle =\ \ \ |\ L=1\ S=1\rangle$

12.2 MeV: $|0_2^+, T=1\rangle = -0.6027|L=0\ S=0\rangle + 0.7980|L=1\ S=1\rangle$

12.8 MeV: $|2_2^+, T=1\rangle = 0.4216|L=2\ S=0\rangle + 0.9068|L=1\ S=1\rangle$.

We note that the Kuo-Lee interaction breaks the Wigner supermultiplet symmetry and selection rules. The Wigner supermultiplet predicts pure L = 2 for the ^{14}N ground state, L = 0 for the 0^+ T = 1 state, and L = 2 for the 2_1^+ state, which would explain the hindrance of the $^{14}C \rightarrow {}^{14}N$ β-decay and the fact that the 2_1^+ state exhausts all the M1 sum rule.[10,40] Our wave functions predict log ft = 5.5, which is greater than the typical Gamow-Teller value (log ft ~ 3) but smaller than the experimentally observed[21] log ft = 9.01. This is not catastrophic, since corrections to the transition operator (exchange currents, second-order forbiddenness, relativistic effects) and expansion of the Hilbert space [e.g. $(sd)^2$ admixtures], which are normally small, become crucial in the case of the present hindered transition.

The calculated ground state magnetic dipole and electric quadrupole moments are 0.34 nm and 13 mb, respectively; the experimental[21] values are 0.40361 nm and 16 ± 7 mb. Cohen and Kurath[40] obtain μ = 0.331 nm. We also calculated BM1 and BE2 rates which are presented in Table IV together with the experimental results. The calculated BM1 rates to the 2_1^+ and 2_2^+ states are 4.877 and 0.041 $(e\hbar/2mc)^2$ respectively, while the experimental rates are 1.44 and 1.53 respectively. The Cohen-Kurath calculation predicts 4.846 $(e\hbar/2mc)^2$ for the transition to the 2_1^+ state. These discrepancies with experiment can be accounted for in terms of sd-shell excitations (see below).

The calculated radiative π-capture rate to the five positive parity states listed above are presented in Table IV. Comparing to the experimental branching ratios (Table I), we see that the calculation describes qualitatively the main features of the spectrum: the weakness of the ground state transition, that the 2_1^+ state is strongest, and that the 1_1^+ state has appreciable strength.

The good quantitative agreement with experiment on the 1_1^+ state is particularly significant, since the studies described below indicate that there is only a 1% $(sd)^2$ component in this state. We note that the (π^-,γ) rate to the 1_1^+ state does not exhibit a close correlation with ^{14}N M1 rates: for example, the theoretical ratios $R_\gamma(1_1^+)/R_\gamma(2_1^+) = 0.2$ is much larger than the corresponding $BM1(1_1^+)/BM1(2_1^+) = 0.016$. This feature is expected for some states since the (π^-,γ) operator is more complex than the M1 operator. Regarding the ground state transition, it is not surprising that the theoretical value $(1.02 \pm 0.2)\times 10^{-4}$ is larger than the measured value $(0.3 \pm 0.2)\times 10^{-4}$, since the ft value was also overestimated. Again, one must bear in mind that small components in the wave function can have large effects on highly hindered (π^-,γ) transitions.

The overestimate of transition strength to the 2_1^+ state can be explained in terms of $(sd)^2$ excitations. Such admixtures to states in ^{14}N were recently calculated[43] in a weak-coupling scheme involving the low-lying eigenstates of the p^{-2}, p^{-4}, and $(sd)^2$ model spaces diagonalized separately in the SU(3) basis. This calculation explains the properties of most of the states below 13 MeV in ^{14}N. It predicts that the 1^+ ground state, 0_1^+ T = 1 and 1_1^+ T = 1 states contain very small $(sd)^2$ admixtures, i.e. 4%, 4%, and 1% respectively. This explains why there is no essential discrepancy between theory and experiment (see Table I) for these states. However, the 2_1^+, 2_2^+ and 0_2^+ states contain large $(sd)^2$ admixtures, i.e. 49%, 56%, and 98%. Since the (π^-,γ) transition operator is in the impulse approximation a 1-body operator, and the ^{14}N ground state is 96% p^{-2}, the $(sd)^2$ admixtures will merely spread the strengths appearing in Table I to more states. Thus, the total strength to the 2_1^+ state, $R_\gamma = 0.96\ (24.3)\times 10^{-4}$, will be divided mainly into two fragments. Taking the above admixtures, this means 51% will go to the 2_1^+ state giving $R_\gamma = 11.9\times 10^{-4}$, and 44% will go to the 2_2^+ state giving $R_\gamma = 10.3\times 10^{-4}$. These results are much closer to the measured distribution of strength

between these two states, i.e., $R_\gamma(2_1^+) = (7.7 \pm 0.9) \times 10^{-4}$ and $R_\gamma(2_2^+) = (4.0 \pm 0.6) \times 10^{-4}$. The summed strength 22×10^{-4} is still higher than the experimental sum $(11.7 \pm 1.1) \times 10^{-4}$.

In the μ-capture reaction $^{14}N(\mu^-, \nu_\mu)^{14}C$, similar discrepancies exist between p^{-2} calculations[44,45] and the measured[46] transition rate to the 2_1^+ state. Using Cohen and Kurath wave functions, Mukhopadyay[44] obtains a value $\sim 2 \times 10^4$ sec^{-1} for the s-state μ-capture rate, which is about twice the experimental value[46] $(1 \pm 0.3) \times 10^4$ sec^{-1}. Thus, by assuming[44,45] ~50% $(sd)^2$ in the 2_1^+ state and ~ 4% $(sd)^2$ in the ^{14}N ground state, one removes the discrepancy with experiment on the 2_1^+ state in both μ- and π-capture. Also, we note that in μ-capture the ^{14}C(g.s.) and 2_2^+ states are predicted to have negligibly weak transition strength and that the 1_1^+ state has ~7% of the 2_1^+ state strength. This distribution of strength in a p^{-2} space correlates closely with our calculations for the (π^-, γ) reaction.

C. Positive Parity States in ^{10}B

The positive parity states which could produce strong (π^-, γ) transitions are those with M1 transitions to the 3^+ ground state of ^{10}B (i.e., 3^+ T = 0, 2^+ T = 1, 3^+ T = 1, 4^+ T = 1) and 0^+ T = 1 and 1^+ T = 1 states. The number of p^6 shell-model components are 10, 14, 7, 4, 7, and 9, respectively. Although the calculation was performed in the j-j coupling scheme, it is more instructive to present the wave functions in the SU(3) scheme, which here coincides with the Wigner supermultiplet scheme:

$$|3^+ \; T=0\rangle = 0.868\,|[42]\,2,1\rangle_1 + 0.285\,|[42]\,2,1\rangle_2 - 0.327\,|[42]\,3,1\rangle + 0.001\,|[42]\,4,1\rangle$$
$$+ 0.150\,|[411]\,3,0\rangle - 0.041\,|[33]\,3,0\rangle + 0.143\,|[321]\,1,2\rangle$$
$$- 0.103\,|[321]\,2,2\rangle + 0.050\,|[321]\,2,1\rangle + 0.047\,|[222]\,0,3\rangle$$

$$|2_1^+\ T=1\rangle = -0.019|[42]\ 2,0\rangle_1 + 0.822|[42]\ 2,0\rangle_2 - 0.272|[411]\ 1,1\rangle$$
$$+ 0.339|[33]\ 1,1\rangle + 0.032|[411]\ 3,1\rangle - 0.297|[33]\ 3,1\rangle$$
$$+ 0.037|[321]\ 1,2\rangle + 0.006|[321]\ 1,1\rangle + 0.112|[321]\ 1,1\rangle_2$$
$$+ 0.055|[321]\ 2,2\rangle - 0.041\ |[321]\ 2,1\rangle + 0.160|[321]\ 2,1\rangle_2$$
$$+ 0.034|[321]\ 2,0\rangle + 0.009|[222]\ 0.3\rangle$$

$$|3^+\ T=1\rangle = 0.909|[42]\ 3,0\rangle - 0.284|[411]\ 3,1\rangle + 0.205|[33]\ 3,1\rangle - 0.041|[321]\ 1,2\rangle$$
$$+ 0.005|[321]\ 2,2\rangle + 0.084|[321]\ 2,1\rangle_1 + 0.207|[321]\ 2,1\rangle_2$$

$$|4^+\ T=1\rangle = -0.617|[42]\ 4,0\rangle + 0.619|[411]\ 3,1\rangle - 0.345|[33]\ 3,1\rangle + 0.248|[321]\ 2,2\rangle$$

$$|0^+\ T=1\rangle = 0.846|[42]\ 0,0\rangle + 0.005|[411]\ 1,1\rangle + 0.500|[33]\ 1,1\rangle + 0.033|[321]\ 1,1\rangle_1$$
$$+ 0.170|[321]\ 1,1\rangle_2 - 0.060|[321]\ 1,1\rangle + 0.001|[222]\ 0,0\rangle.$$

For the higher excited 2^+ states we get

2_2^+: E_x = 4.7 MeV C_i: 0.857, 0.089, -0.109, -0.398, 0.175, -0.126, -0.099, 0.053, 0.124, 0.065, 0.082, -0.030, -0.021, -0.036

2_3^+: E_x = 7.0 MeV C_i: -0.422, 0.126, -0.263, -0.671, -0.098, -0.240, -0.317, 0.191, -0.179, 0.150, 0.114, 0.041, -0.085, -0.071

where the C_i are the coefficient of each basis vector in the same order as for the 2_1^+ state. The basis states are indicated in the standard notation $|[f]L,S\rangle$, where [f] = permutation symmetry of the spatial wave function. {In SU(3) notation[47] [42] = (2,2), [411] = (3,0), [33] = (0,3), [321] = (1,1), [222] = (0,0).} The above eigenstates do not have a simple structure in the Wigner supermultiplet scheme, partly because the additional quantum number required to distinguish the two [42] L = 2 states does not have physical meaning. The M1, E2, and (π^-,γ) rates obtained from the above wave functions are given in Tables III and IV.

The magnetic and quadrupole moments of the 3^+ T=0 ground state are 1.9 nm and 0.056, respectively. The experimental values are 1.8 nm and

0.086. Thus we expect the ^{10}B ground state wave function to be fairly reliable.

We find that nearly all M1 strength is exhausted below 12 MeV (Table III) with 91% of the strength going to three states (2_2^+, 2_3^+, 3_1^+) out of a possible 25. In the SU(3) basis, it is not easy to see why the 2_2^+ state exhausts most of the M1 sum rule (47%, Table III) while the 2_1^+ state is weak (1%). Cohen and Kurath obtain 1.812 nm for the ground state and BM1 values of 2.786, 0.665, 1.521, and 0.244 $(e\hbar/2mc)^2$ for the 2_2^+, 2_3^+, 3_1^+, and 4_1^+ states, respectively

The comparison with experimental (π^-,γ) branching ratios (Table II) is most significant on the lowest three states in ^{10}Be, since the experimental branching ratios should be quite accurate. For these three states, 0_1^+, 2_1^+, 2_2^+, the calculated relative distribution of strength 1/2.4/4.7 is in excellent agreement with the experimental relative branching ratios of $1/1.8 \pm 0.41/4.2 \pm 0.8$. The calculated absolute values are too high by factors of 1.4 to 1.9. The overall theoretical normalization is affected by the choice of $\hbar\omega$ (radial p-shell wave function), distortion factors C_s and C_p, and the 1s and 2p strong-absorption level widths which are used to obtain branching ratios from transition rates. The cumulative error from uncertainties in these quantities could account for discrepancies of the size obtained.

The μ-capture reaction $^{10}B(\mu^-,\nu_\mu)^{10}Be$ was studied with the Cohen-Kurath model by Mukhopadyhay.[12] Unfortunately the μ-capture measurements have not been performed. Comparing the predicted distribution of μ-capture strength with the R_γ of Table IV, one sees that the 2_2^+ state dominates both reactions. A significant difference is obtained for the 3_1^+ (T=1) state, estimated to be between 7 and 9 MeV in ^{10}Be. It is the second strongest state in μ-capture with 34% of the 2_2^+ state strength, but weakly excited in (π^-,γ) with 9% of the 2_2^+ state branching ratio.

D. Negative Parity States in ^{14}N

Within the chosen model space there are 20, 50, 56, 43, and 24 shell-model components in the 0^-, 1^-, 2^-, 3^-, and 4^- T=1 subspaces, respectively.[48] The calculated wave functions for the 0^-, 1^-, and 2^- states have already been checked in a study[37] of the $^{13}C(p,\gamma)^{14}N$ reaction. The experimental E1 spectrum is described fairly well. The main concentration of strength is predicted in 2^- states at 21.3 MeV and 1^- states at 21.5 MeV in ^{14}N. In the $^{13}C(p,\gamma_0)^{14}N$ reaction[25] the peaks are seen at 22.5 and 23.0 MeV in ^{14}N, and much of the strength was associated with 2^- states. The calculations also predict 2^-, 1^-, and 0^- strength at higher energies.

In comparing photonuclear and (π^-,γ) transitions to negative parity states in the GDR region, one must bear in mind that the E1 operator of photoexcitation does not explicitly depend on the spin and has strong "non-spin-flip" matrix elements (e.g., p3/2→ d5/2 etc.). However, the (π^-,γ) operator depends on the nucleon spin (except for the very weak D-term) and has strong "spin-flip" matrix elements (e.g., 1p3/2 → 1d3/2). Thus one expects the collective state observed in photoexcitation to contain predominantly "non-spin-flip" excitations, while the collective states observed in (π^-,γ) reaction must contain predominant "spin-flip" excitations. For a $J^\pi = 1^+$ target such as ^{14}N, the (π^-,γ) reaction can have strong transitions to 3^- states though the dipole operator, i.e., an operator with L = 1, S = 1, J = 2, and T = 1. Such states cannot be excited in photoabsorption via E1 transitions.

The energy separations of isospin and spin-isospin dipole vibrations are generally not well known. For the simpler case of ^{16}O, we calculated the excitation energies using the Kuo-Brown interaction, with the result: $E_x \approx 23.0$ MeV for the ordinary GDR (isospin wave), $E_x \approx 27.0$ MeV for the 1^- T=1 spin-isospin GDR, and $E_x \approx 21.0$ MeV for the 2^- T=1 spin-isospin resonance. The situation in ^{14}N is more complex because the above three

vibrations are mixed by recouplings arising from the Pauli principle.

The calculated branching ratios for ^{14}N are presented graphically in Fig. 7. The strongest states are: $J^{\pi}(R_{\gamma}$ in %) E_x in MeV = $3^-(0.06)14.7$, $2^-(0.10)$ 16.0, $3^-(0.06)$ 16.7, $3^-(0.12)$ 17.0, $3^-(0.25)$ 17.5, $1^-(0.07)$ 18.1, $2^-(0.05)$ 18.8, $2^-(0.12)$ 19.7, and $2^-(0.06)$ 23.9. We see that the strongest transitions due to 1^-, 2^-, and 3^- final states are predicted at 18.1, 19.7, and 17.5 MeV, respectively. As in photoexcitation, the calculated energies are lower by several MeV than the peaks in the spectra (Fig. 7a). The total radiative branching ratio to all negative parity states is 1.95%, with 0.06% to 0^- states, 0.42% to 1^- states, 0.66% to 2^- states, 0.73% to 3^- states, and 0.07% to 4^- states.

A more complete comparison of the calculated distribution of negative parity excitations with the (π^-, γ) data is given in Fig. 7b. To obtain the curves on this figure we (a) assigned each theoretical level a BW shape with fwhm = 1 MeV, (b) shifted all E_x up by 2.5 MeV to conform approximately to the photoexcitation study,[37] (c) folded the theoretical spectrum ($R_s + R_p$ vs E_{γ}) with the instrumental line shape and detection efficiency (Fig. 2), and (d) normalized the theoretical spectrum to the number of stopped pions. The resulting spectrum was multiplied by 0.4 to approximately fit the data in the GDR region. Thus the figure corresponds to $R_{\gamma} = 0.4 \times 1.95 = 0.78\%$ for the calculated negative parity states.

The factor of 0.4 is somewhat arbitrary. Clearly a factor < 1 is needed since the calculated branching ratio of 1.95% to $1\hbar\omega$ excitations is almost equal to the measured $2.13 \pm 0.21\%$ for all transitions. One expects appreciable strength to other excitations, e.g., $0\hbar\omega$, $2\hbar\omega$, and quasi-free (QF). If the $1\hbar\omega$ states are associated with the BW contribution obtained in the fit to the data with the pole-model + BW ($R_{\gamma} = 0.21 \pm 0.02\%$), a reduction factor of 0.1 is needed.

The central question is how to separate resonance and QF capture. Our wave functions for the negative parity states are not orthogonal to the wave functions of the same J^{π} obtained by coupling the (A-1) nuclear wave functions with those of an unbound neutron moving in an optical potential. Therefore, our computed rates include a certain amount of QF cross section. However, it is difficult to see how these amounts can be large, since when one expands the distorted optical-potential wave functions for an unbound neutron in an harmonic oscillator basis, it is seen that the $1\hbar\omega$ components are small.[49]

Other uncertainties in the calculations result from the use of pionic orbit distortion factors (Sec. IVA) derived from the bound-state calculations involving only p-shell nucleons, and from the use of harmonic oscillator wave functions for unbound nucleons. It seems reasonable that errors here could lead to factors of 2 in the total $1\hbar\omega$ rates, but factors of 10 seem improbable.

It is clear that the excitation of continuum states needs a more precise theoretical treatment. Nevertheless, from the above comparisons with the ^{14}N data, it seems reasonable to conclude the 3^- states are indeed strongly excited. A similar calculation[50] for the $^{6}Li(\pi^-,\gamma)^{6}He$ reaction also indicated that 3^- states would be strongest, and some evidence for a peak ($E_x \approx 23$ MeV) was seen in the data.[3,51] These results, if corroborated by further investigations, demonstrate an attractive feature of the (π^-,γ) reaction, viz., that collective spin-isospin dipole vibrations with $J_f = J_i + 2$ are preferably excited. Such states are difficult to observe in other reactions and cannot be formed in E1 photoexcitation.

V. CALCULATION OF 1s-RADIATIVE CAPTURE TRANSITION TO THE ^{14}C(g.s.) IN THE "ELEMENTARY-PARTICLE SOFT-PION" ANSATZ

The $^{14}N(\pi^-, \gamma)\ ^{14}C$(g.s.) transition rate from 1s-state capture may be calculated following the treatment of Delorme[52] for the similar $^{6}Li(\pi^-, \gamma)$ ^{6}He(g.s.) transition, which is also a $1^+ \rightarrow 0^+$ transition. Delorme obtains the expression

$$\Lambda_\gamma(1s;\ 1^+ \rightarrow 0^+) = \frac{(1.22e)^2}{6\pi^2 f_\pi^2}\ C_s (Z\,\alpha\, m'_\pi)^3\, k \left(1 - \frac{m_\pi}{4m_i}\right) \frac{1}{4m_i^2}\ F_A^2(q^2) \qquad (7)$$

with $e^2 = 4\pi\alpha$, $f_\omega = 0.932\ m_\pi$, k = photon momentum = 138.6 MeV, q^2 = (4-momentum transfer)^2 = 0.489 F^{-2} for the $^{14}N \rightarrow\ ^{14}C$ transition, m'_π = reduced pion mass, m_i = mass (^{14}N), Z = 7; $\hbar = c = 1$. The factor 1.22, which was 1.35 in Delorme's original calculation, comes from the more recent work of Ericson and Rho;[9] it represents the corrections for ρ exchange, incoherent rescattering and nuclear intermediate states. The distortion of the pion wave function due to the strong interaction in the initial state is taken into account by the multiplicative factor $C_s = 0.50$ (Section IVA).

The axial-vector form factor for the pure $1^+ \rightarrow 0^+$ GT transition is determined by assuming[9] that its variation with q^2 between 0 and 0.489 F^{-2} is the same as that of the electromagnetic form-factor $F_M(q^2)$ of the M1 transition ^{14}N(g.s.) $\rightarrow\ ^{14}N$ (2.313 MeV), where the latter state is the analog of ^{14}C(g.s.). $F_A^2(0)$ is determined from the β-decay ft value[53] 1.052×10^5 sec. Using the expression given by Delorme

$$\frac{F_A^2(0)}{4m_i^2} = \frac{2\pi^3 \ln 2}{3\, G^2 m_e^5 ft_{1/2}} \qquad (8)$$

we obtain $F_A^2(0)/4m_i^2 = 1.978 \times 10^{-6}$.

Ensslin et al.[54] measured the $^{14}N(e,e')\ ^{14}N(2.313\ MeV)$ transition and obtain the following parametrization of $F_M(q^2)$:[55]

$$F_M(q^2) = 0.01226\ e^{-0.7627\ q^2}[(0.40 \pm 0.06) + (0.823 \pm 0.071)q^2], \qquad (9)$$

which gives $$F_M(489\ F^{-2})\ /F_M(0)| = 1.38 \pm 0.12.$$

Taking this value for $F_A(q^2 = 0.489\ F^{-2})/F_A(q^2 = 0)$, we obtain $\Lambda_\gamma(1s;\ 1^+ \rightarrow 0^+) = 1.31 \times 10^{11}\ sec^{-1}$.

The radiative capture branching ratio for 1s capture then is

$$R_s = \frac{\Lambda_\gamma(1s;\ 1^+ \rightarrow 0^+)}{\Lambda a\ (1s)}\ \omega_s = \frac{1.31 \times 10^{11}\ sec^{-1}}{6.82 \times 10^{18}\ sec^{-1}} \times 0.1 = 1.9 \times 10^{-9}.$$

This value is considerably smaller than the 2.9×10^{-5} obtained in the shell-model calculation (Sec. IVB). We note that the shell-model calculation yields log ft 1/2 = 5.5 instead of the experimental value log ft 1/2 = 9. We see that if the assumed variation of $F_A(q^2)$ with q^2 is correct, the soft-pion prediction gives an extremely small 1s-radiative capture branching ratio. Thus the measured value, $R_\gamma = (3 \pm 2) \times 10^{-5}$, if different from zero, must be explained in terms of p-state capture.

VI. CONCLUSIONS

Some of the conclusions that we can draw from this study of the (π^-, γ) reaction with stopped pions on ^{14}N and ^{10}B are:

(1) The (π^-, γ) reaction on p-shell nuclei selectively excites the analogs of giant M1 states of the target. The data on ^{14}N and ^{10}B, and those of previous studies on ^6Li and ^{12}C, clearly demonstrate that the strongest (π^-, γ) transitions correspond to such excitations. The successful measurement and analyses of these transitions most clearly establish the (π^-, γ) reaction as a quantitative probe of nuclear structure.

(2) The calculations of the (π^-,γ) transition rates for 1s and 2p capture, in terms of an IA Hamiltonian and shell-model wave functions obtained using realistic interactions, yielded satisfactory agreement with our measurements. In ^{14}N there is good agreement on the strongest transitions (2_1^+ and 1_1^+ states) if one includes the $(sd)^2$ admixtures in excited states required by other data on the same states. In ^{10}B, branching ratios for three states could be measured accurately due to the wide level separations. The shell-model calculation in a p^6 vector space predicts the relative branching ratios to these three states correctly, but overestimates the absolute values by ~ 1.7

(3) The interesting transition $^{14}N(\pi^-,\gamma)\,^{14}C(g.s.)$ is very weak, as was anticipated from the $\sim 10^6$ hindrance of the β-decay between the same two states. The shell-model calculations overestimate both the (π^-,γ) and β-rates although small values are predicted. The PCAC and soft-pion calculation for the 1s radiative capture yields a negligibly small branching ratio. Thus the observed strength, $R_\gamma = (3\pm2)\times10^{-5}$, if not equal to zero, must arise from p-state capture. The small experimental upper limit determines that even the p-state radiative transition rate is small; perhaps this transition can be used in future studies extending soft-pion theorems to p-state capture.

(4) The ^{14}N data give evidence for excitations of spin-isospin dipole vibrations at 20 ± 1 MeV in ^{14}C. The shell-model calculations suggest that the predominant contributions are from 2^- and 3^- states, with the 3^- states strongest. This contrasts with E1 photoexcitation where 1^- and 2^- states dominate and 3^- states cannot be excited. Thus the (π^-,γ) reaction, by exciting spin-isospin dipole vibrations with $J_f = J_i + 2$, provides complementary information in the study of continuum states in the GDR region.

ACKNOWLEDGMENTS

The authors wish to express their gratitude to Drs. C. Werntz, N. Mukhopadhyay, G. Nixon, and L. Fagg for enlightening discussions on various aspects of this study. The cooperation and assistance given by Leal Kanstein and the members of the 184-inch cyclotron crew are much appreciated. The assistance given by Dennis Soon and Victor Elischer in various aspects of this experiment are gratefully acknowledged.

FOOTNOTES AND REFERENCES

†Work performed under the auspices of the U. S. Atomic Energy Commission.

*Present address: Dept. of Physics, Case Western Reserve Univ., Cleveland, Ohio 44106

‡Permanent address: DPHN/HE, C.E.N. SACLAY, BP N°2, 91-Gif sur Yvette, France.

1. P. Truöl, H. W. Baer, J. A. Bistirlich, K. M. Crowe, N. de Botton, and J. A. Helland, Phys. Rev. Lett. 32, 1268 (1974).

2. J. A. Bistirlich, K. M. Crowe, A. S. L. Parsons, P. Skarek, and P. Truöl, Phys. Rev. Lett. 25, 950 (1970).

3. H. W. Baer, J. A. Bistirlich, K. M. Crowe, N. de Botton, J. A. Helland, and P. Truöl, Phys. Rev. 8 C, 2029 (1973).

4. J. A. Bistirlich, K. M. Crowe, A. S. L. Parsons, P. Skarek, and P. Truöl, Phys. Rev. Lett. 25, 689 (1970).

5. J. A. Bistirlich, K. M. Crowe, A. S. L. Parsons, P. Skarek, and P. Truöl, Phys. Rev. C 5, 1867 (1972).

6. H. W. Baer, J. A. Bistirlich, N. de Botton, S. Cooper, K. M. Crowe, P. Truöl, and J. D. Vergados, Phys. Rev. 10 C, 0000 (1974).

7. H. Überall, Acta Physica Austriaca 30, 89 (1969).

8. J. D. Walecka, Preludes in Theoretical Physics, edited by A. de Shalit, H. Feshback, and L. Van Hove (Interscience, New York, 1966).

9. For a recent review see M. Ericson and M. Rho, Phys. Reports 5, 57 (1972), and A. Figureau in Proc. International Seminar on π-Meson Nucleus Interactions, Strasbourg, 1971 (Université Louis Pasteur, Strasbourg, France, 1971).

10. D. Kurath, Phys. Rev. 130, 1525 (1963).

11. For references and a review see L. W. Fagg, International Conf. on Photonuclear Reactions and Applications, Asilomar, California, 1973, edited by B. L. Berman (Lawrence Livermore Laboratory CONF-730301, 1973), p. 663.

12. N. C. Mukhopadhyay, Phys. Lett. 45B, 309 (1973).

13. J. D. Vergados and H. W. Baer, Phys. Lett. 41B, 560 (1972).

14. N. C. Francis and K. M. Watson, Amer. J. Phys. 21, 659 (1953).

15. G. Giocomelli, P. Pini, and S. Stagni, CERN-HERA 60-1 (CERN, Geneva, 1969).

16. P. Spillantini and V. Valente, CERN-HERA 70-1 (CERN, Geneva, 1970); V. Rossi, A. Piazza, G. Sussino, F. Carbonara, G. Gialanella, M. Napolitano, R. Rinzivillo, L. Votano, G. C. Mantovani, A. Piazzoli, and E. Loddi-Rizzini, Nuovo Cimento 13A, 59 (1973).

17. We used Eqs. (2) and (3) of the article by E. Garwin, W. Kernan, C. O. Kim and C. M. York, Phys. Rev. 115, 1295 (1959).

18. H. Hilscher, W.-D. Krebs, G. Sepp, and V. Soergel, Nucl. Phys. A158, 602 (1970).

19. L. G. Dakhno and Yu. D. Prokoshkin, Sov. J. Nucl. Phys. 7, 351 (1968); a more general discussion in the context of dispersion theory for direct nuclear interactions is given by I. S. Shapiro, Selected Topics in Nuclear Theory, edited by F. Janouch (IAEA, Vienna, 1963), p. 85 ff.

20. H. W. Baer and K. M. Crowe, Int. Conf. on Photonuclear Reactions and Applications, Asilomar, California, 1973, edited by B. L. Berman (Lawrence Livermore Laboratory CONF-730301, 1973), p. 583 ff.

21. F. Ajzenberg-Selove, Nucl. Phys. A152, 1 (1970); also 1973 updated compilation (private communication).

22. H.-G. Clerc and E. Kuphal, Z. Phys. 211, 452 (1968).

23. G. C. Ball and J. Cerny, Phys. Lett. 21, 551 (1966).

24. R. W. Gellie, K. H. Lokan, N. K. Sherman, R. G. Johnson, and J. I. Lodge, Can. J. Phys. 50, 1689 (1972), and references quoted therein; H. R. Kissener, R. A. Eramzhian, and H.-U. Jäger, Nucl. Phys. A207, 78 (1973).

25. F. Riess, W. J. O'Connell, and P. Paul, Nucl. Phys. A175, 462 (1971).

26. B. L. Berman, Atlas of Photoneutron Cross Sections Obtained with Monoenergetic Photons, UCRL-74622 (1973).

27. T. Lauritsen and F. Ajzenberg-Selove, Nucl. Phys. 78, 1 (1966); also, lemon aid preprint series, Cal. Tech. publication LAP-124, 1974.

28. E. Spamer, Z. Phys. 191, 24 (1966).

29. R. J. Hughes and B. M. Spicer, Int. Conf. on Photonuclear Reactions and Applications, Asilomar, California, 1973, edited by B. L. Berman (Lawrence Livermore Laboratory CONF-730301, 1973), p. 153.

30. G. A. Fisher (Ph.D. dissertation), Stanford University, 1970; results on GDR region of ^{10}B are quoted in Ref. 27.

31. G.F. Chew, M.L. Goldberger, F.E. Low, Y.Nambu, Phys.Rev. 106, 1345 (1957).

32. J. Delorme and T. E. O. Ericson, Phys. Lett. 21, 98 (1966).

33. References and tabulation are given in Ref. 20.

34. F.A. Berends, A.Donnachie, D.L. Weaver, Nucl.Phys. B4, 1 (1967).

35. W. Maguire and C. Werntz, Nucl. Phys. A205, 211 (1973).

36. M. Krell and T.E.O. Ericson, Nucl. Phys. B11, 521 (1969).

37. J. D. Vergados, Univ. of Pennsylvania Preprint UPR-0031N, 1974 (Nucl. Phys., in press).

38. S. Y. Lee, Theory of Effective Interactions and Operators in Nuclear Structure (Ph.D. dissertation, SUNY, at Stony Brook, 1972).

39. T. T. S. Kuo and G. E. Brown, Nucl. Phys. 85, 40 (1966); ibid. A92, 481 (1967).

40. S. Cohen and D. Kurath, Nucl. Phys. 73, 1 (1965).

41. W. W. Sapp, M. Eckhause, G. H. Miller, and R. E. Welsh, Phys. Rev. C 5, 690 (1972).

42. References to original work and comparison of various measurements and optical potential calculations are given by G. Backenstoss, Annual Rev. Nucl. Sci. 20, 467 (1970).

43. S. Lie, Nucl. Phys. A181, 517 (1972).

44. N. C. Mukhopadhyay, Phys. Lett. 44B, 33 (1973).

45. V. A. Vartanyan, T. A. Dmitrieva, H.-U. Jäger, G. R. Kissener, and R. A. Eramzhyan, Sov. J. Nucl. Phys. 11, 295 (1970).

46. Results of Dubna group quoted in Ref. 45.

47. J. D. Vergados, SU(3) Techniques for Shell Model Studies and the Spectra of A = 25 Nuclei (Ph.D. dissertation), University of Michigan, 1968 (unpublished).

48. There are 11 additional states (one 0^-, five 1^-, three 2^-, and two 3^-, T = 1 states) which correspond to the center-of-mass motion of the nucleus as a whole. These spurious states, mixed via the interaction with the non-spurious states, were found to affect significantly the energies and (π^-, γ) strengths of the negative parity states. Hence they were projected out using standard techniques.

49. Calculations dealing with this point are being performed in collaboration with T.-S.H. Lee and will be published separately.

50. J. D. Vergados, Nucl. Phys. A220, 259 (1974).

51. The 3^- identification (Ref. 50) for a resonance centered at $E_x \approx 23$ MeV in ^{6}He is further supported by the recent observation of such a state in the mirror nucleus ^{6}Be by E. Ventura, J. Calarco, C. C. Chang, E. M. Diener, E. Kuhlmann, and W. E. Meyerhof, Nucl. Phys. A219, 157 (1974).

52. J. Delorme, Nucl. Phys. B19, 573 (1970).

53. R. W. Kavanagh, Nucl. Phys. A129, 172 (1969).

54. N. Ensslin, W. Bertozzi, S. Kowalski, C. P. Sargent, W. Turchinetz, C. F. Williamson, S. P. Fivozinsky, J. W. Lightbody, and S. Penner, Phys. Rev. 9 C, 1705 (1974).

55. F_M of Delorme[52] = F_{M1}/q of Ensslin et. al.[54]

TABLE I. Energies and branching ratios for transitions in the $^{14}N(\pi^-,\gamma)$ reaction with stopped pions.

E_γ (MeV)	Γ (MeV)	$E_x(^{14}C)$[a] (MeV)	$E_x(^{14}N)$[b] (MeV)	J^π	R_γ(expt.) (10^{-4})	R_γ(theory)[c,d] (10^{-4})
138.1	0	0	2.31	0^+	0.3 ± 0.2	1.02 ± 0.14
131.1	0	7.0 ± 0.1	9.17	2^+	7.7 ± 0.9[e]	24.3 ± 2.7
129.8	0	8.32	10.43	2^+	4.0 ± 0.6	1.2 ± 0.2
126.9	0	11.3	13.75	1^+	5.1 ± 0.7	4.9 ± 0.7
118.2 ± 1.0	2.4 ± 0.5	20.0 ± 1.0	22.2	(3^-)[f]	20.5 ± 2.0[g]	195 ± 22[h]
Pole (Δ = 13.5 MeV)					176 ± 18	
Total					213 ± 21	227 ± 25[i]

[a] Energies from previous work,[21] except for 7.0 MeV state and BW at 20 MeV.

[b] Energies for analog states in ^{14}N.

[c] Obtained from $R_\gamma = [C_s\omega_s\lambda_\gamma(1s)/\lambda_a(1s)] + [C_p\omega_p\lambda_\gamma(2p)/\lambda_a(2p)]$ with $\omega_p = 0.90 \pm 0.03$, $\omega_s = 1-\omega_p$, $C_s = 0.5$, $C_p = 1.4$(text), $\lambda_a(1s) = 4.48 \pm 0.30$ keV/$\hbar$, and $\lambda_a(2p) = 2.1 \pm 0.3$ eV/$\hbar$ (Ref. 42); uncertainties indicated are due to x-ray data only.

[d] Assumed $(p3/2, p1/2)^{-2}$ configurations for positive parity states. For some states $(sd)^2$ excitations are important (Sec. IVB).

[e] If assume a single line at E_x = 7.3 MeV, $10^4 R_\gamma = 10.3 \pm 1.7$.

[f] Dominant J^π value expected from theory (text).

[g] Fit with Δ = 13.5 MeV (Fig. 3d); separation of pole and BW not well defined; other fits show variations of 30% are possible.

[h] 0^-, 1^-, 2^-, 3^-, 4^-, states based on 1 $\hbar\omega$ excitations (text).

[i] Sum of strength to p^{-2} and $1\hbar\omega$ excitations (text).

TABLE II. Energies and branching ratios for transitions in the $^{10}B(\pi^-, \gamma)$ reaction with stopped pions.

E_γ (MeV)	$E_x(^{10}Be)$[a] (MeV)	$E_x(^{10}B)$[b] (MeV)	J^π	R_γ(expt.) (10^{-4})	R_γ(theory)[c,d] (10^{-4})
137.4	0	1.74	0^+	2.5 ± 0.4	3.6 ± 0.7
134.1	3.37	5.11	2^+	4.4 ± 0.7	8.5 ± 1.7
131.6	5.96	7.48	2^+	10.5 ± 1.3	16.9 ± 2.7
130.2	7.55	8.89	2^+		6.5 ± 1.0
128.9 ± 0.7	8.6 ± 0.7	~ 9.7	(4^+) [e]	10.6 ± 1.6[f]	2.7 ± 0.4
127.4 ± 0.7	10.1 ± 0.7	~ 11.5	(3^+) [e]		1.4 ± 0.2
Pole (Δ = 13.0 MeV)				198 ± 23	
Total				227 ± 22	

[a] Energies and J^π of lowest four states are from previous work.[27]

[b] Energies on analog states in ^{10}B.

[c] Obtained from $R_\gamma = [C_s \omega_s \lambda_\gamma(1s)/\lambda_a(1s)] + [C_p \omega_p \lambda_\gamma(2p)/\lambda_a(2p)]$ with $\omega_p = 0.80 \pm 0.05$, $\omega_s = 1 - \omega_p$, $C_s = 0.5$, $C_p = 1.4$ (discussed in text), $\lambda_a(1s) = 1.68 \pm 0.12$ keV/$\hbar$ (Ref. 42) and $\lambda_a(2p) = 0.32 \pm 0.06$ eV/$\hbar$ (Ref. 42); uncertainties indicated are due to x-ray data only.

[d] Assuming $(p3/2, p1/2)^6$ configurations.

[e] Dominant J^π values expected from theory (Sec. IVC).

[f] Values for individual states cannot be determined reliably from our data; values corresponding to curves of Fig. 5 are $R_\gamma(8.6) = 0.049 \pm 0.01\%$, $R_\gamma(10.1) = 0.058 \pm 0.010\%$.

TABLE III. M1 and E2 transition rates $^{14}N[1^+ T = 0(g.s) \rightarrow J^\pi T = 1]$ and $^{10}B[3^+ T = 0(g.s.) \rightarrow J^\pi T = 1]$. Configurations p^{-2} (^{14}N) and p^6 (^{10}B) are assumed.

^{14}N	Theory	Expt.[a]	Theory		
J^π	E_x (MeV)	BM1 $(e\hbar/2mc)^2$	BM1 $(e\hbar/2mc)^2$	% of sum	BE2 e^2F^4
0_1^+	1.5	0.019 ± 0.003	0.096	2	
2_1^+	6.5	1.44 ± 0.17	4.877	93	0.919
1_1^+	8.5		0.077	1	2.679
0_2^+	13.7	0.05	0.140	3	
2_2^+	14.2	1.53 ± 0.19	0.041	1	0.356
^{10}B					
2_1^+	3.0	0.10	0.065	1	0.026
2_2^+	4.7		2.702	47	0.013
2_3^+	6.9		1.838	32	0.223
3_1^+	7.4		0.697	12	0.287
3_2^+	11.0		0.144	3	0.447
3_3^+	12.9		0.065	1	0.190
4_1^+	9.0		0.013	0	0.771

[a] Reference 21 for ^{14}N, Ref. 27 for ^{10}B.

TABLE IV. Theoretical (π^-, γ) transition rates and branching ratios for 1s and 2p capture in ^{14}N and ^{10}B. For ^{10}B only the strong states are included.

J^π	T	E_x[a] (MeV)	$\Lambda_\gamma(1s)$ (10^{16}sec^{-1})	$\Lambda_\gamma(2p)$ (10^{12}sec^{-1})	R_s (10^{-4})	R_p (10^{-4})	R_γ[b] (10^{-4})
^{14}N							
0^+	1	0.0	0.3963	0.1856	0.291	0.730	1.02
0^+_2	1	12.2	0.1621	0.1875	0.119	0.738	0.86
2^+_1	1	5.0	7.5624	4.7509	5.561	18.707	24.33
2^+_2	1	12.7	0.1811	0.2661	0.133	1.048	1.18
1^+_1	1	7.0	0.8281	1.0789	0.609	4.248	4.86
^{10}B							
0^+_1	1	0.0	0.0707	0.1426	0.277	3.278	3.56
2^+_1	1	2.6	0.1985	0.3351	0.778	7.706	8.48
2^+_2	1	4.3	1.4949	0.4777	5.862	10.986	16.85
2^+_3	1	6.5	0.4400	0.2052	1.725	4.719	6.45
4^+_1	1	8.6	0.1741	0.0881	0.623	2.025	2.71
4^+_3	1	14.1	0.2906	0.1397	1.140	3.212	4.35
3^+_1	1	7.0	0.1148	0.0431	0.450	0.992	1.44

[a] Theoretical value for energy in residual nucleus (^{14}C and ^{10}Be) relative to ground state. The identification with experimental levels (Table I,II) is on the basis of J^π.

[b] Results are for p^{-2} and p^6 configurations; the effects of $(sd)^2$ excitations are important for some states, as discussed in text.

FIGURE CAPTIONS

Fig. 1. Plan view of the experimental setup. The insert shows the e^+ - e^- pair spectrometer and range-telescope geometry. The trigger for an event is $\pi 1 \times \pi 2 \times \pi 3 \times \overline{\pi s} \times \overline{\pi c} \times (A \times B)_i \times (A \times B)_k$, $i \neq k, k \pm 1$.

Fig. 2. (a) Efficiency of the pair spectrometer as a function of photon energy; η = conversion probability $\times$ $(\Delta\Omega/4\pi)$ $\times$ detection efficiency. (b) Photon spectrum of π-capture on hydrogen. The distortion of the rectangular shape of the π^0 spectrum is due to the reduction in efficiency at the low-energy end.

Fig. 3. Photon energy spectrum from π-capture on ^{14}N. (a) Raw data for stopped-π capture. (b) Photon spectrum for pions with mean energy of 44 MeV used for in-flight background subtraction. (c) Spectrum after in-flight subtraction. The solid line is the spectrum calculated from the one-pole diagram (insert) representing quasi-free capture.[19] Evidence for resonance excitation at $E_\gamma \approx 118$ MeV can be seen. (d) Fit to the data with pole-model + Breit-Wigner + 4 lines. The transition to ^{14}C(g.s.) is seen to be extremely weak. The strongest transition is to the analog of the giant M1 state of ^{14}N at 9.17 MeV.

Fig. 4. Photon spectrum from capture of stopped pions on ^{10}B. (a) Raw data. (b) Spectrum after small in-flight subtraction. The solid line is the spectrum calculated from the one-pole diagram (insert) representing quasi-free capture.[19] (c) Fit to the data with pole-model + 5 lines. Dashed lines show the contributions of the first three states of ^{10}Be. The strongest transition is to the 2_2^+ state, which is the analog of the giant M1 state in ^{10}B at 7.48 MeV.

Fig. 5. Photon spectrum and level diagram for (π^-, γ) transitions to the particle-stable and low-continuum states of ^{14}C. The spectrum is after subtraction of the pole-model and BW contribution (Fig. 3d). The strong

M1 transitions observed in 180° electron scattering are identified. The M1 transition to ^{14}N(13.8 MeV) has not yet been looked for in 180° electron scattering.

Fig. 6. Photon spectrum and level diagram for (π^-, γ) transitions to the particle-stable and low-continuum states of ^{10}Be. The spectrum is after subtraction of the pole-model contribution (Fig. 4c). The first three levels of ^{10}Be are clearly resolved. The transition strength to higher levels is not resolved, but two lines were sufficient to fit the data. The M1 transition to the 7.5-MeV state dominating 180° electron scattering is indicated on the level diagram; the analog state is seen to dominate the (π^-, γ) spectrum.

Fig. 7. Results of the shell-model calculation for $1\hbar\omega$ negative parity excitations in the reaction ^{14}N(π^-, γ) ^{14}C are compared to the data. (a) Branching ratios to the strongest states. The data are on an arbitrary scale. (b) Theoretical transition strength ($\times$ 0.4) folded with the instrumental resolution and efficiency. A level width of 1 MeV (BW shape) was assigned to each level. It is seen that the peak in the data at $E_x(^{14}C)$ = 20 MeV is predicted to arise from strong excitation of 3^- spin-isospin dipole states.

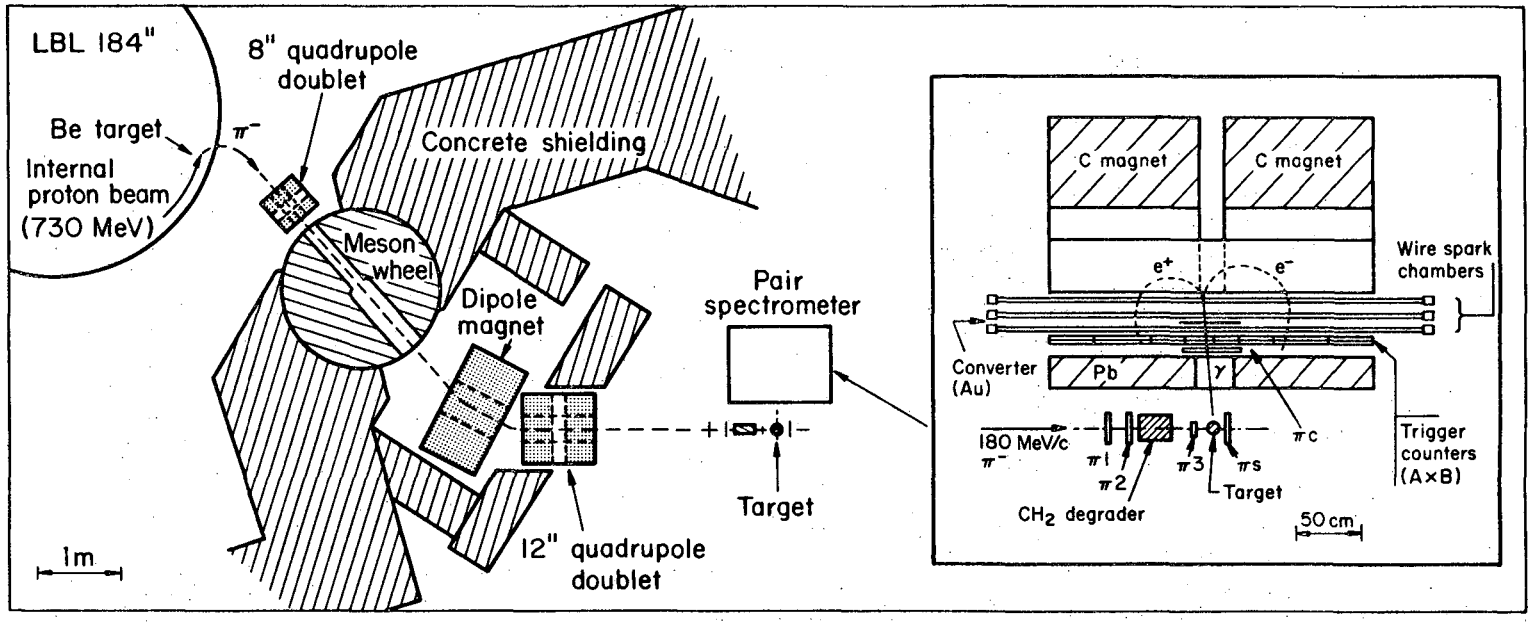

XBL 747-3689

Fig. 1

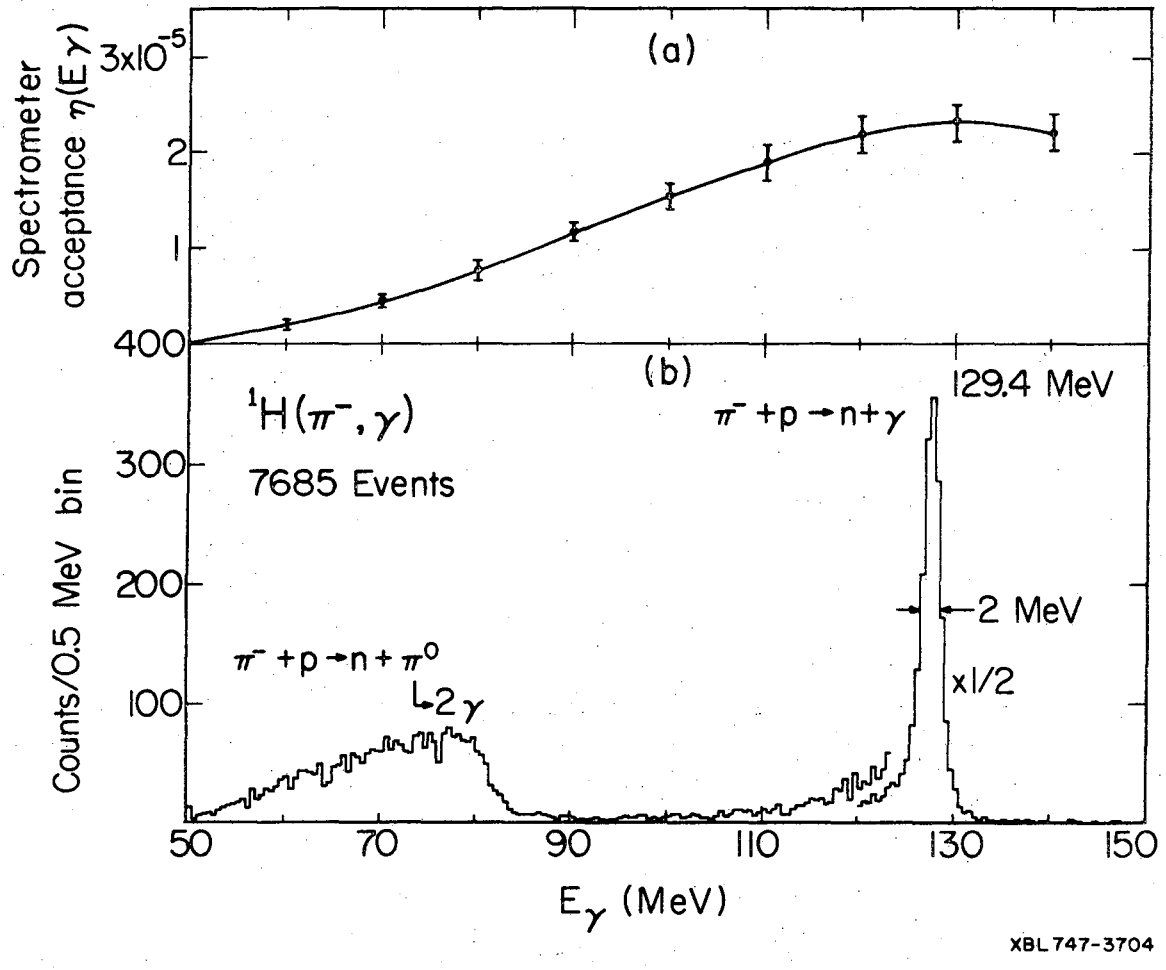
(a)
Spectrometer acceptance η(Eγ)
3x10⁻⁵
2
1
400
(b)
¹H(π⁻, γ)
7685 Events
π⁻ + p → n + γ
129.4 MeV
2 MeV
x1/2
π⁻ + p → n + π⁰
↳2γ
Counts/0.5 MeV bin
300
200
100
50
70
90
110
130
150
Eγ (MeV)
XBL747-3704

Fig. 2.

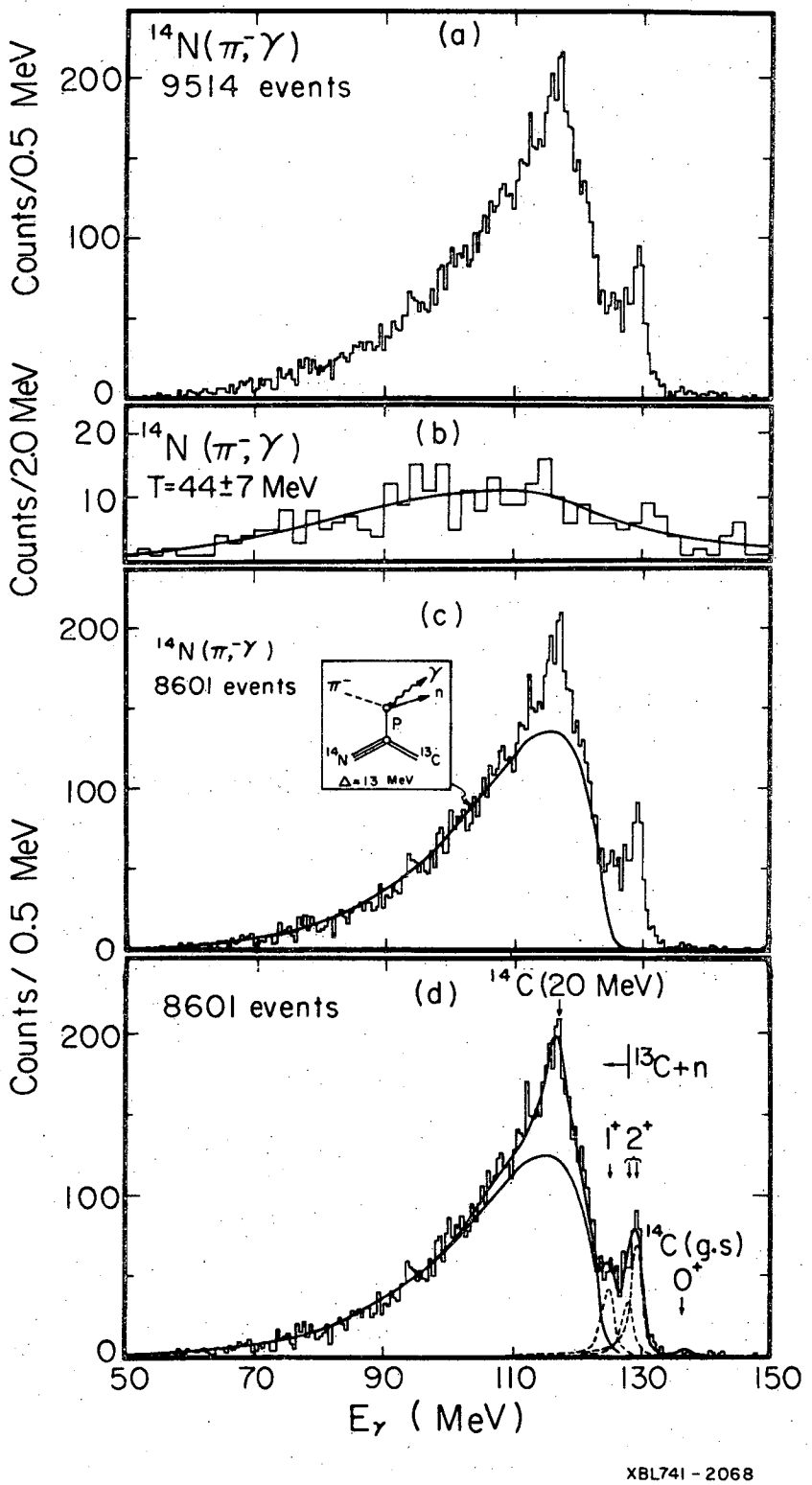
$^{14}N(\pi^-,\gamma)$
9514 events
(a)
Counts/0.5 MeV
200
100
0
$^{14}N(\pi^-,\gamma)$
T=44±7 MeV
(b)
Counts/20 MeV
20
10
$^{14}N(\pi^-,\gamma)$
8601 events
(c)
π^-
γ
n
P
^{14}N
^{13}C
Δ=13 MeV
Counts/ 0.5 MeV
8601 events
(d)
^{14}C(20 MeV)
$^{13}C+n$
1^+ 2^+
^{14}C(g.s)
0^+
50
70
90
110
130
150
E_γ (MeV)
XBL741-2068

Fig. 3.

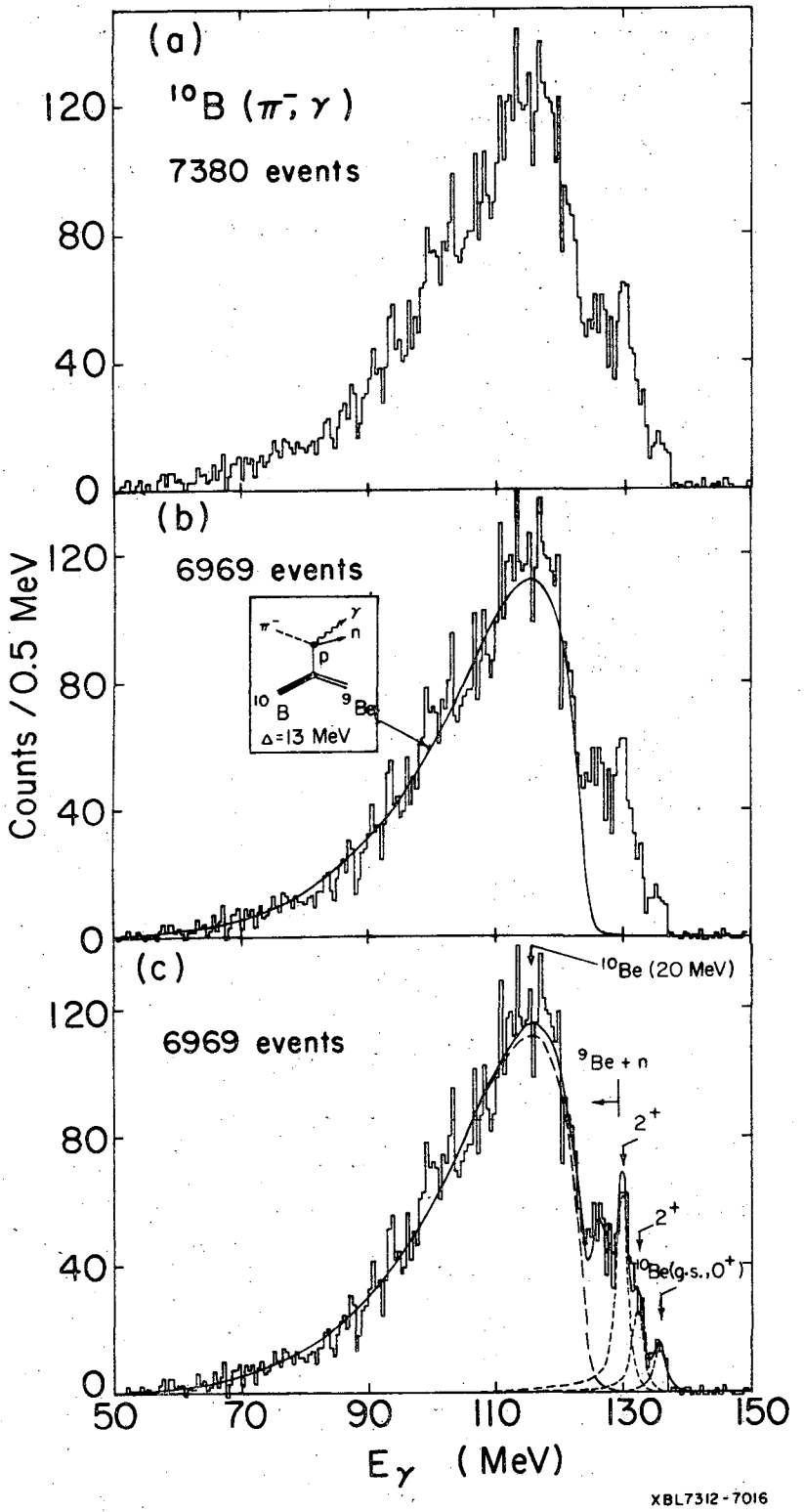
(a)
$^{10}B(\pi^-,\gamma)$
7380 events
(b)
6969 events
π^-
γ
n
p
^{10}B
^{9}Be
Δ=13 MeV
(c)
6969 events
^{10}Be (20 MeV)
$^{9}Be + n$
2^+
2^+
$^{10}Be(g.s.,0^+)$
Counts /0.5 MeV
E_γ (MeV)
XBL7312-7016

Fig. 4.

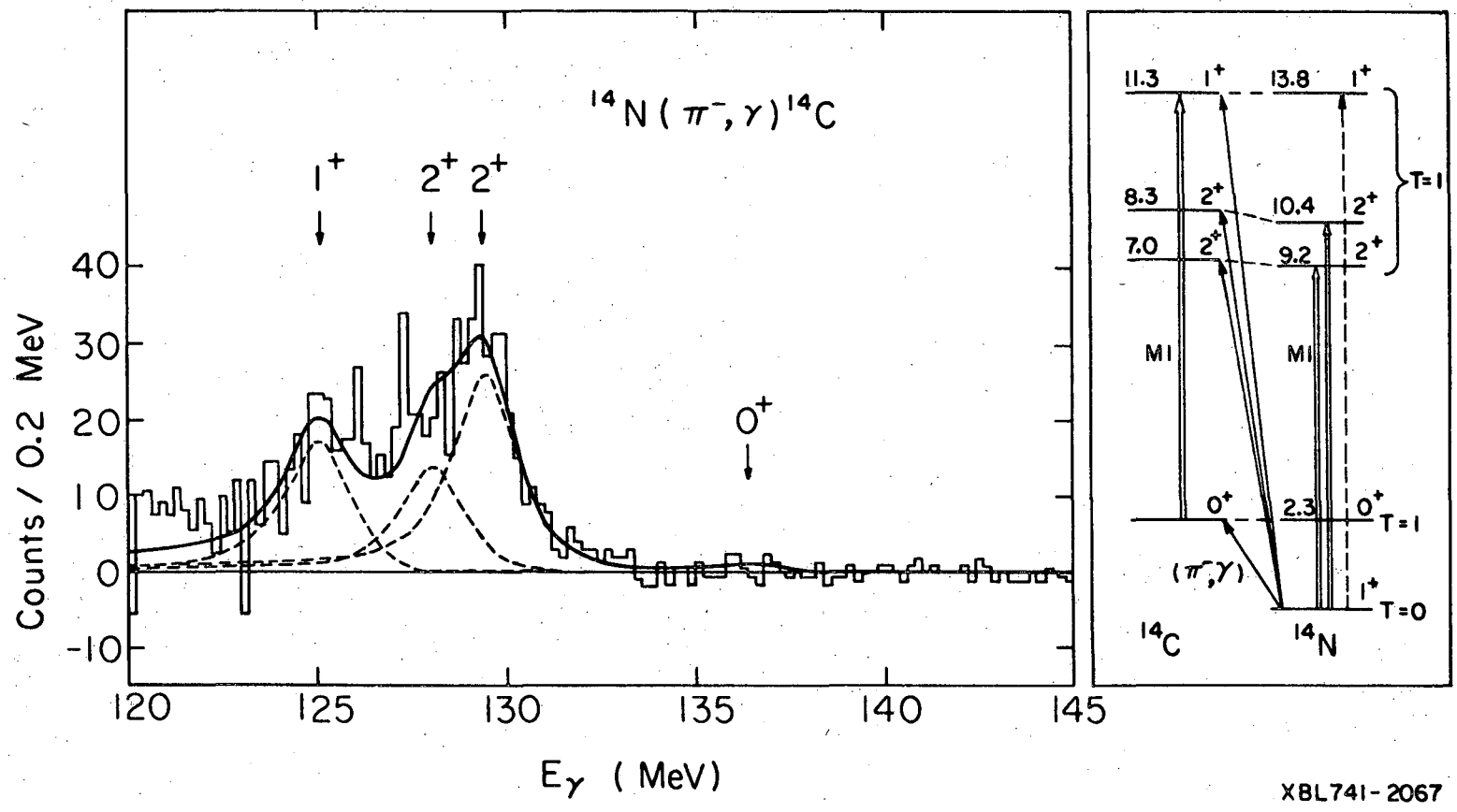
$^{14}N(\pi^-,\gamma)^{14}C$
1^+
2^+ 2^+
0^+
Counts / 0.2 MeV
40
30
20
10
0
-10
120
125
130
135
140
145
E_γ (MeV)
11.3 1^+
13.8 1^+
T=1
8.3 2^+
10.4 2^+
7.0 2^+
9.2 2^+
M1
M1
0^+
2.3 0^+ T=1
(π^-,γ)
1^+ T=0
^{14}C
^{14}N
XBL741-2067

Fig. 5

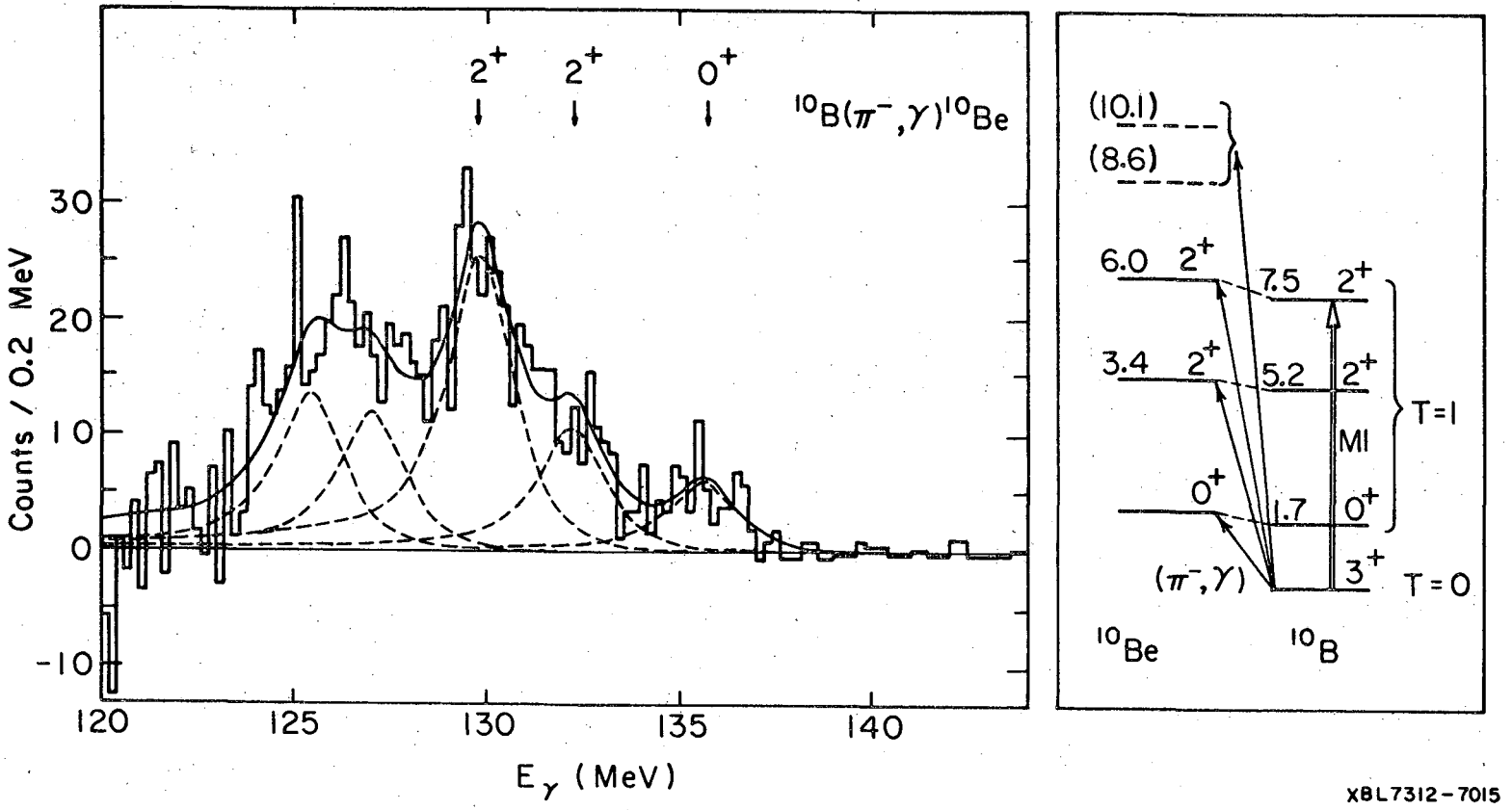
2+
2+
0+
10B(π−,γ)10Be
Counts / 0.2 MeV
30
20
10
0
-10
120
125
130
135
140
Eγ (MeV)
(10.1)
(8.6)
6.0 2+
7.5 2+
3.4 2+
5.2 2+
M1
T=1
0+
1.7
0+
(π−,γ)
3+
T=0
10Be
10B
XBL7312-7015

Fig. 6

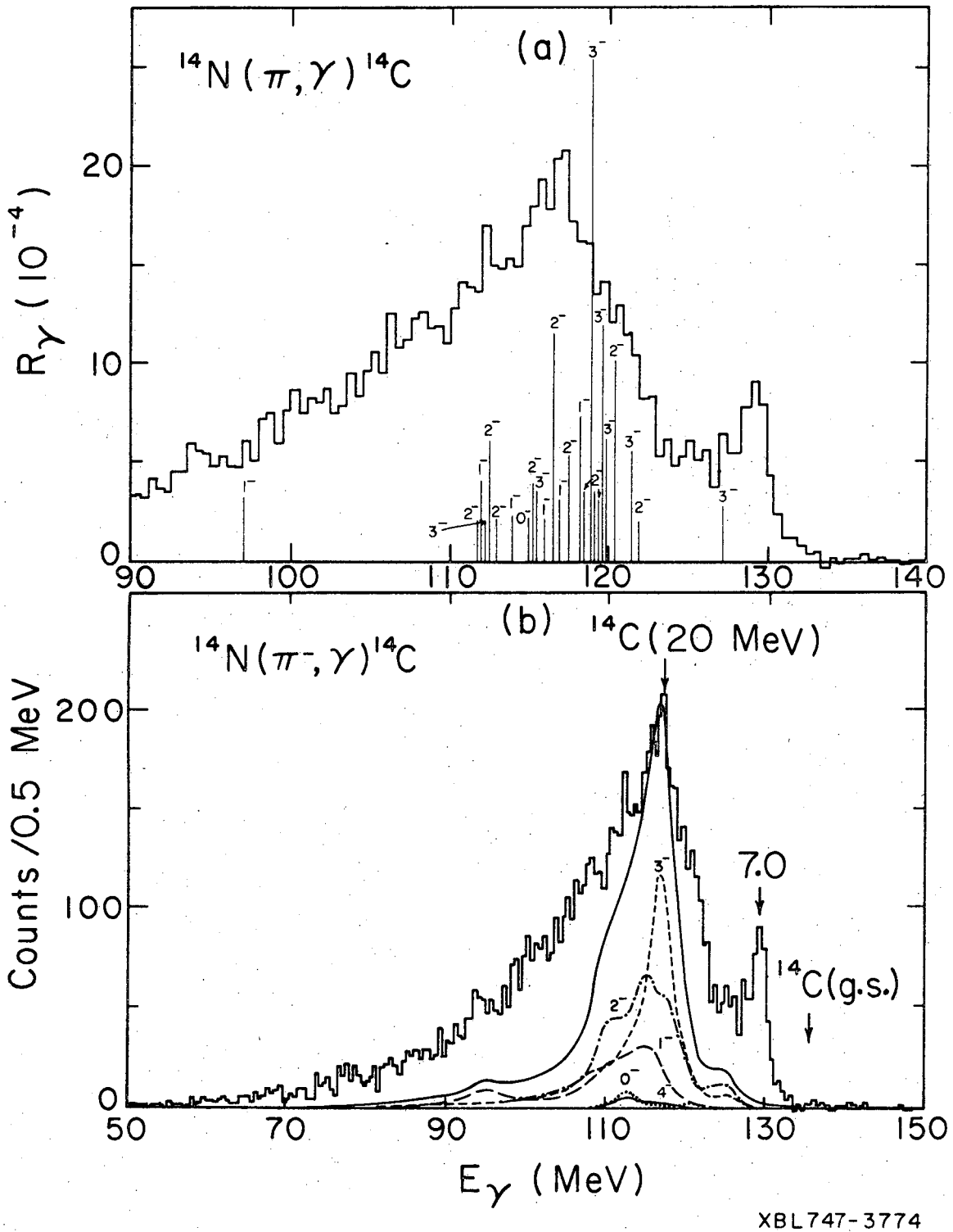
(a)
$^{14}N(\pi,\gamma)^{14}C$
R_γ (10^{-4})
20
10
0
90
100
110
120
130
140
(b)
$^{14}N(\pi^-,\gamma)^{14}C$
^{14}C(20 MeV)
7.0
^{14}C(g.s.)
Counts/0.5 MeV
200
100
0
50
70
90
110
130
150
E_γ (MeV)
XBL747-3774

Fig. 7.

TECHNICAL INFORMATION DIVISION
LAWRENCE BERKELEY LABORATORY
UNIVERSITY OF CALIFORNIA
BERKELEY, CALIFORNIA 94720